Design and Analysis of a Hybrid Diffractive/Refractive Achromat for use in Optical Data Storage

by

David A. Kubalak

Submitted in Partial Fulfillment
of the
Requirements for the degree

MASTER OF SCIENCE

Supervised by Professor G. Michael Morris

The Institute of Optics
University of Rochester
Rochester, New York

1993

Acknowledgments

First and foremost, I would like to thank my advisor, G. Michael Morris. I am extremely grateful and fortunate for having received his guidance and support–both during my undergraduate years, and while completing this work. I would also like to thank the members of Prof. Morris' group, especially Dan Raguin, Scott Norton, Alan Heaney, and Don Miller for the many discussions, particularly on Wednesday afternoons. Also in my gratitude are Len Saaf, Dean Faklis, and Dale Buralli for their advice and assistance; Gayle Thompson for having all the answers; and Yasuhiro Yoshitake, for pointing out how lucky we are.

I would also like to thank Dave Kay, of Eastman Kodak, for providing me with much information regarding optical data storage systems, and for assisting me with fabrication.

My parents deserve much gratitude for their constant support and encouragement, and I would like to thank Corinna Lathan for always being there, even though I wished she was here.

I would also like to acknowledge the support provided by the University of Rochester, Institute or Optics, New York Center for Advanced Optical Technology, and the U.S. Army Research Office.

Abstract

The design and analysis of a hybrid diffractive/refractive achromat for optical data storage is presented, beginning with a discussion of the construction and diffraction efficiency of surface-relief diffractive lenses. The phase function, which defines a diffractive lens in much the same manner as a surface sag equation defines a refractive lens, is examined. The thin lens, or Sweatt, model of a diffractive lens is discussed, and equations are provided that allow conversion to and from the phase model. The thin lens model provides a good method to design diffractive lenses using conventional lens design software. This model also provides a convenient means of deriving the third-order aberrations of a diffractive lens.

A wave propagation approach is used to discuss how decentering or tilting one of the elements with respect to the other will affect the PSF and MTF of a doublet. Two examples of achromat design are presented. First, a conventional refractive achromat with no spherical aberration or coma is designed, and the method is then extended to design a hybrid diffractive/refractive achromat.

Finally, design constraints and performance goals for a hybrid diffractive/refractive achromat for use in an optical data storage system is presented. Two figures of merit used to evaluate the performance of the achromat are the Strehl ratio, which should remain greater than 0.96 over a 1° half field of view, and the ratio of focal length change per wavelength change, which should remain less than 0.1μm/nm over the wavelength band. An optimized hybrid achromat is presented, and design tolerances with respect to fabrication errors—element misalignment, thickness errors, diffractive surface zone radii errors, blaze height errors, and mask misalignment errors—are discussed.

Table of Contents

List of Tables

List of Figures

1. Introduction

1.1. Brief history of hybrid achromats

1.1.1. Preface

The purpose of this thesis is to investigate the use of a surface-relief diffractive optical element in conjunction with a conventional refractive element to produce a hybrid diffractive/refractive achromat for use in optical data storage. Since the invention of the diffraction grating in 1785 by David Rittenhouse, there have been, of course, many developments in the theory and use of diffractive optical elements. This chapter provides a description of work performed in the area of achromatization with diffractive optical elements.

1.1.2. Earlier work

Early work in the area of surface relief diffractive optics was provided by Sliusarev,[1] Tudorovskii,[2] and Miyamoto.[3] Sliusarev discussed the profile shape required for producing only on focus, and included a description of the "phase plates" dispersion. Tudorovskii approximated the desired continuous profile with discrete steps and considered inserting a phase plate into an optical system to correct chromatic aberration. Miyamoto also considered the spectral characteristics of "phase Fresnel lenses" and investigated their ability to form aspheric wavefronts.

Madjidi-Zolbanine and Froehly[4] discussed the use of a holographic optical element (HOE) to correct both chromatic and spherical aberrations of glass lenses. They proposed two methods for making the HOE: recording the interference pattern formed by two point sources, and recording the interference pattern formed by the aberrated wavefront formed by an optical system and the desired wavefront.

In 1988, Stone and George[5] investigated the use of holographic optical elements with conventional glass elements to form a hybrid element with an arbitrary Abbe ν-number. As a special case, they considered hybrid achromats ($\nu = \infty$) and three-element hybrid apochromats. Faklis and Morris[6] provided a Fresnel diffraction analysis of an imaging system containing three lenses of arbitrary dispersion. As a special case, they described a system using holographic lenses to produce a well-corrected image in broadband visible light. Twardowski and Meyrueis[7] considered plano-convex and plano-concave singlets with HOEs recorded in a coating on the plane surface. They also provide a method of designing the optimal HOE for any singlet hybrid system.

Diffractive lenses have been used with success in the infrared region. Swanson and Veldkamp[8] used a diffractive surface to correct both chromatic and spherical aberration in the infrared region, thus eliminating the need for costly aspherics or an additional refracting element. Foo, et.al.,[9] Fritz and Cox,[10] and Wood[11] provided numerous design examples.

1.2. Overview of thesis

Chapter 2 addresses some of the basic ideas needed to design optical systems with surface-relief diffractive elements. Section 2.2 includes a description of the surface-relief structure, beginning with how it is constructed from the desired phase modulation, and ending with a discussion of diffraction efficiency. The thin lens, or "Sweatt model" of a diffractive lens is presented in Section 2.3. The thin lens model provides a convenient means to design diffractive elements on conventional lens design software. Aspheric wavefronts are considered, and equations are given which can be used to convert between aspheric coefficients for the thin lens model, and higher order phase coefficients in the phase function representation. It is also shown how the thin lens model can be used to derive the Seidel aberrations of a diffractive lens.

Chapter 3 discusses the use of diffractive surfaces to achromatize refractive elements. In Section 3.2, the results in Chapter 2 are used to analyze the effects of aberrations on the point spread (PSF) and modulation transfer function (MTF) of an achromat. It is shown how aberrations in one element of a doublet can be used to cancel aberrations in the other element. The elements of a doublet can be decentered or tilted with respect to one another during fabrication and the affects of these fabrication errors are also considered in Section 3.2. It is shown how both decenter and tilt produce a shift in the coordinates of the image, and how this shift is proportional to the magnitude of the error. It is also shown how the aberrations in the elements of decentered or tilted achromats no longer cancel. Section 3.3 provides two examples of achromat design. The first is a conventional cemented achromat. With careful choice of glasses, it is seen that it is possible to design a cemented achromat with no spherical or coma. An example of a hybrid achromat is then considered. It is necessary to use the fourth-order phase coefficient to correct spherical aberration, but with both bending parameters remaining as degrees of freedom, a solution is readily found for a cemented hybrid achromat with no

spherical or coma. It is also shown that the curvatures on the glass element of a hybrid achromat will be much less than on the crown element of the conventional achromat. Spherochromatism is also considered, and seen to have a large effect on the PSF of the hybrid lens.

Chapter 4 considers the application of hybrid diffractive/refractive achromats to optical data storage (ODS) systems. Section 4.2 presents the design constraints and performance goals. Design constraints include entrance pupil diameter, f/number, working distance, and field of view. Design goals include a polychromatic Strehl ratio greater than 0.96 over the full field, and a focal length change per wavelength change of less than 0.1μm/nm over the wavelength band. A hybrid achromat meeting these requirements is presented, and fabrication methods are discussed. Section 4.3 describes common errors which may arise during fabrication. First, errors which affect the image quality are considered, these include element misalignment and thickness errors, and diffractive surface zone shrinkage. It is shown that the lens performs well within the capabilities of existing technology. Next, errors which affect the diffraction efficiency are discussed, including etch depth errors, and mask misalignment.

1.3. References for chapter 1

1. G. G. Sliusarev, "Optical systems with phase layers," Sov. Phys. Dokl **2,** 161-163 (1957).
2. A. Tudorovskii, "An objective with a phase plate," Opt. and Spect. **2,** 126-133 (1959).
3. K. Miyamoto, "The phase Fresnel lens," J. Opt. Soc. Am. **51,** 17-20 (1961).
4. H. Madjidi-Zolbanine, C. Froely, "Holographic correction of both chromatic and spherical aberrations of single glass lenses," Appl. Opt. **18,** 2385-2393 (1979).
5. T. Stone, N. George, "Hybrid diffractive-refractive lenses and achromats," Appl. Opt. **27,** 2960-2971 (1988).
6. D. Faklis, G. M. Morris, "Broadband imaging with holographic lenses," Opt. Eng. **28,** 592-598 (1989).
7. P. Twardowski, P. Meyrueis, "Design of some achromatic imaging hybrid diffractive-refractive lenses," *Holographic Optics III: Principles and Applications*, Proc. SPIE, **1507,** pp. 55-65 (1991).
8. G. J. Swanson, W. B. Veldkamp, "Diffractive optical elements for use in infrared systems," Opt. Eng. **28,** 605-608` (1989).
9. L. D. Foo, S. P. Clark, R. T. Mercado, "Design examples of hybrid refractive-diffractive lenses," *Current Developments in Optical Engineering and Commercial Optics*, Proc. SPIE, **1168,** pp. 117-125 (1989).
10. T. A. Fritz, J. A. Cox, "Diffractive optics for broadband infrared imagers: design examples," *Holographic Optics: Optically and Computer Generated*, Proc. SPIE, **1052,** pp. 25-31 (1989).
11. A. P. Wood, "Using hybrid refractive-diffractive elements in infrared Petzval objectives," Proc. SPIE, **1354**, (1990).

Chapter 2

2. Diffractive lenses

2.1. Introduction

A diffractive lens, known in the literature as a kinoform,[1, 2] binary lens,[3, 4, 5] phase Fresnel lens,[6] or simply as a phase plate,[7, 8] introduces a phase modulation across the surface of the wavefront such that light passing through the lens will constructively interfere at the focal point. This thesis is concerned with rotationally symmetric diffractive lenses in which the phase modulation is introduced by a surface relief profile. The depth of profile is chosen such that the maximum phase modulation is 2π at the design wavelength. The shape of the profile is chosen to yield the highest efficiency possible in the design order.

Diffractive lenses have many advantages which make them an attractive choice to lens designers. One advantage is their extremely high, negative, dispersion.[9] This unique quality, which usually limits the use of diffractive elements to narrow bandwidths, allows new possibilities for the achromatization of lenses.[6–10, 11] Hybrid achromats tend to be lighter and smaller then conventional achromats and offer the possibility of lower f/numbers. Additionally, achromatization with a diffractive surface eliminates the need for exotic glasses. Achromats made from common glasses such as BK7 and a diffractive surface perform very well.[9] Hybrid lenses are especially attractive in the infrared region, where conventional materials are limited and can be expensive. [12]

Another important feature is that diffractive lenses with the stop in contact have zero field curvature and distortion. With a stop shift, coma and astigmatism can be eliminated.[13] Efficient diffractive lenses can be replicated from a master, thus eliminating the need to polish glass elements. This is especially important considering

the fact that aspheric wavefronts can be produced by diffractive lenses with little increase in complexity.

Section 2.2 outlines the construction and diffraction efficiency of surface relief diffractive lenses, including the phase function. The phase function defines a diffractive lens in much the same manner in which a surface sag equation defines a refractive lens. Section 2.3, describes the thin lens model of a diffractive lens. The thin lens model provides a method of designing diffractive lenses on conventional lens design software, even if the software is not designed to handle diffractive optics. The thin lens model also provides a convenient means to derive the third order aberrations of diffractive lenses.

2.2. Surface-Relief Diffractive Lenses

2.2.1. Surface-Relief Structure

To construct a surface-relief diffractive lens, we recall that full period Fresnel zones are spaced such that the optical path length from the edge of the j^{th} zone to the focal point is equal to $f_0+j\lambda_0$, where λ_0 is the design wavelength, and f_0 is the desired focal length, as in Fig. 2.2.1.

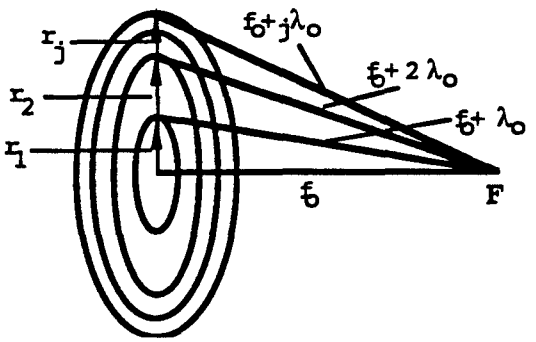

Fig. 2.2.1. Full-period Fresnel zone construction. The edge of each zone is one wavelength, λ_0, further from the focal point F than the edge of the preceding zone.

The radii of the exact Fresnel zones are given by

$$r_j^2 = 2j\lambda_o f_o + (j\lambda_o)^2, \tag{2.2.1}$$

but in the paraxial region, where $(j\lambda/4f_0) << 1$, the radii of the j^{th} zone can be given by

$$r_j = \sqrt{2j\lambda_o f_o}\ . \tag{2.2.2}$$

To create a diffractive lens, material is added in each zone and the thickness of this material is varied to introduce the correct amount of phase modulation such that all the light passing through the structure constructively interferes at the focal point.

The correct surface-relief profile is obtained from the phase transmission function, $\varphi(r)$, by noting that the OPD introduced by the lens is OPD = $(\lambda_o/2\pi)|\varphi(r)|$. Also, OPD = $[n_s(\lambda_o) - 1]d(r)$, where n_s is the index of the material, and d(r) is thickness of the material at the radius r. By combining these two equations, we find that

$$d(r) = \left(\frac{\lambda_o}{2\pi}\right)\frac{|\varphi(r)|}{n_s(\lambda_o)-1}. \tag{2.2.3}$$

If the maximum phase to be introduced by the lens is 2π, then the maximum surface height is

$$d_{max} = \frac{\lambda_o}{n(\lambda_o)-1}. \tag{2.2.4}$$

Dammann[14] and Buralli, et. al.[15] showed that for a phase function described here as

$$\varphi(r) = 2\alpha\pi\left(j - \frac{r^2}{2\lambda_o f_o}\right), \qquad \text{for } r_j \le r < r_{j+1}, \tag{2.2.5}$$

where the parameter α is the dephasing due to wavelengths other than the design wavelength λ_o, or

$$\alpha = \frac{\lambda_o[n(\lambda)-1]}{\lambda[n(\lambda_o)-1]}, \tag{2.2.6}$$

a change of variables $\xi = r^2/(2\lambda_o f_o)$ transforms the phase function into

$$\varphi(\xi) = \alpha 2\pi(j - \xi) \qquad \text{for } j \le \xi < j+1. \tag{2.2.7}$$

Furthermore, since the transmission function, $t(\xi) = \exp[i\varphi(\xi)]$, is now periodic, it can be expressed as a Fourier series, ie:

$$t(\xi) = \exp\left[i\varphi(\xi)\right] = \sum_{m=-\infty}^{\infty} c_m \exp(i2\pi m\xi) \tag{2.2.8}$$

where

$$c_m = \frac{\exp[-i\pi(\alpha+m)]}{\pi(\alpha+m)}\sin[\pi(\alpha+m)]\,. \tag{2.2.9}$$

We would like positive values of f, and positive orders of m to correspond to converging diffracted orders. Therefore, we change m to -m and reverse the order of summation. The result, with the reverse substitution for ξ, is

$$t(r) = \sum_{m=-\infty}^{\infty} \exp[-i\pi(\alpha-m)]\sin c(\alpha-m)\exp\left(\frac{-i\pi m r^2}{\lambda_o f_o}\right), \tag{2.2.10}$$

where

$$\sin c(x) \equiv \frac{\sin(\pi x)}{\pi x}\,. \tag{2.2.11}$$

By comparing Eq. (2.2.10) with the Fourier optics definition of a transmission function for a refractive lens,[16] ie:

$$t(r)_{\text{thin lens}} = \exp\left(\frac{-i\pi r^2}{\lambda f}\right), \tag{2.2.12}$$

the diffractive lens is seen to behave like a refractive lens with an infinite number of focal lengths:

$$f_{\text{diff lens}} = \frac{\lambda_o f_o}{m\lambda}. \tag{2.2.13}$$

In general the phase function $\varphi(r)$ can be written as

$$\varphi(r) = 2\pi\left(Ar^2 + Dr^4 + Er^6 + Fr^8 + Gr^{10} + \ldots\right), \tag{2.2.14}$$

where A, D, E,... are the higher order phase coefficients. Until now, we have only been discussing the paraxial regime, where

$$A = \frac{1}{2\lambda_o f_o} \tag{2.2.15}$$

and the higher order coefficients are all zero. The paraxial diffractive lens described above, therefore, has a parabolic blaze. Giving value to the higher order coefficients varies the zone spacing, and has the same effect as adding aspherics to a refractive surface–that is, the higher order phase coefficients can be used to correct field aberrations.

2.2.2. Diffraction Efficiency

Diffraction efficiency is a measure of how much of the incident light constructively interferes at the desired focal point. Light that does not interfere constructively at the focal point manifests itself as background light (or noise) in the focal plane, and decreases the MTF of the lens.

For a paraxial diffractive lens with a quadratic blaze, the diffraction efficiency is given by[15]

$$\eta(\lambda, m) = c_m c_m^* = \sin c^2(\alpha - m), \qquad (2.2.16)$$

where c_m is defined in Eq. (2.2.9). The design order is the first diffracted order, m = 1, and from Eq. (2.2.16), the diffractive lens is seen to be 100% efficient when the design wavelength is used, i.e., when $\alpha = 1$. For a diffractive lens made of PMMA, Eq. (2.2.16) takes the form shown in Fig 2.2.2.

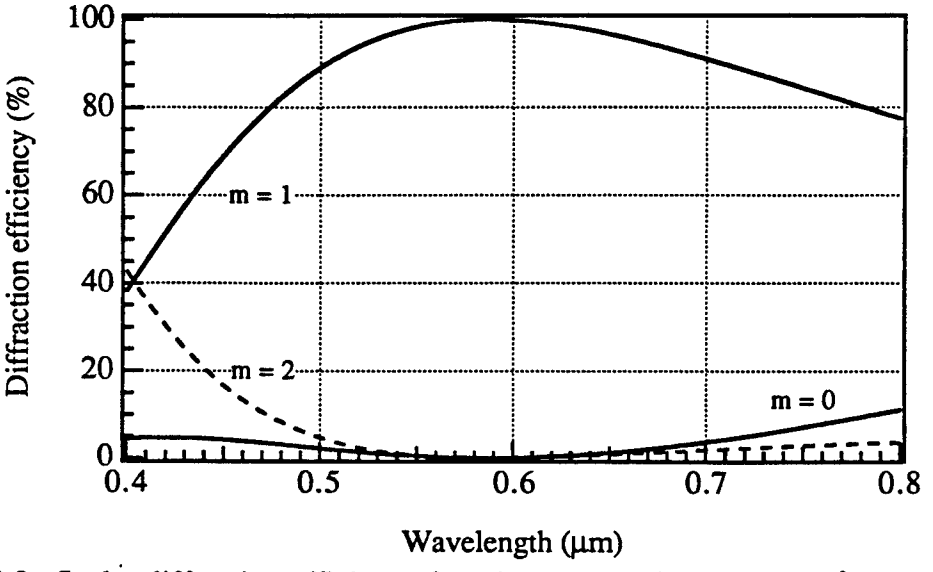

Fig. 2.2.2. Scalar diffraction efficiency for a lens made of PMMA. As λ varies from the design wavelength, λ_o, the efficiencies in the m=0 and m=2 orders increase.

If wavelengths other than the design wavelength are incident on the lens, then the efficiency in the design, or first, order decreases, and the efficiencies in the 0^{th} and 2^{nd} orders increase.

Frequently, the quadratic blaze is approximated with a staircase, as in Fig. . The phase function for a staircase profile with p steps is described as[14]

$$\varphi(r) = \frac{2\alpha\pi}{p}(p - k), \qquad (2.2.17)$$

for $$\frac{kd}{p} \le r \le \frac{(k+1)d}{p}, \qquad k = 0, 1, 2, \ldots p - 1,$$

where d is a period and α is defined by Eq. (2.2.6). The diffraction efficiency can be found by again describing Eq. (2.2.17) as a Fourier series and proceeding in the same manner as above. The result is

$$\eta(\alpha, p, m) = \frac{\sin^2\left(\frac{\pi m}{p}\right)\sin^2[\pi(\alpha - m)]}{(\pi m)^2 \sin^2\left[\frac{\pi}{p}(\alpha - m)\right]}, \tag{2.2.18}$$

where, again, m is the order number. For a multi-level diffractive lens made of PMMA, Eq. (2.2.18) takes the form shown in Fig. .

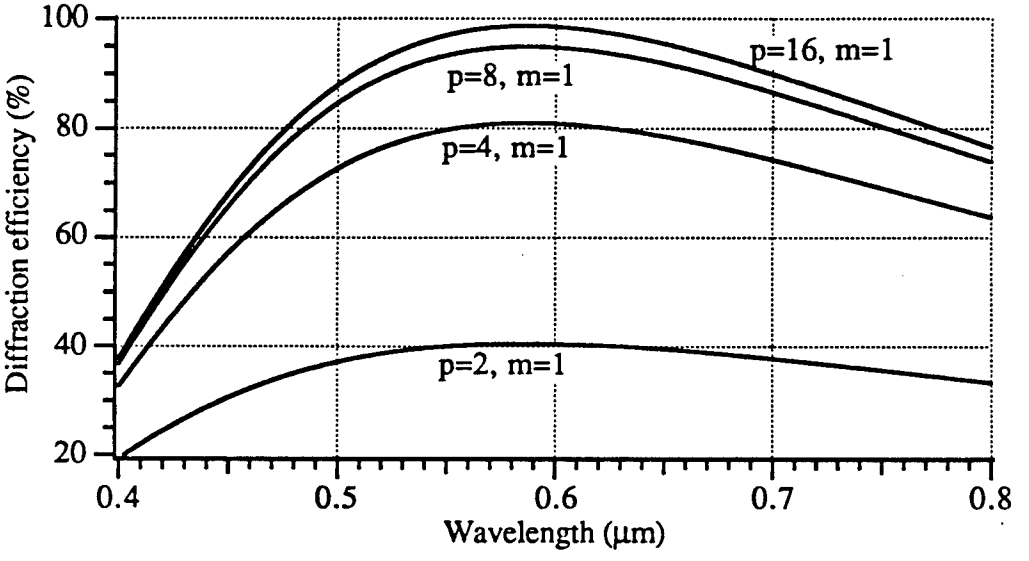

Fig. 2.2.3 Scalar diffraction efficiencies for multi-level lenses made fo PMMA. The diffraction efficiency increases with the number of steps, p.

For $\alpha = 1$, Eq. (2.2.18) can be greatly simplified to yield

$$\eta(p,m) = \frac{\sin c^2\left(\frac{1}{p}\right)}{m^2}, \quad \text{when } m-1 = g \bullet p,$$

and (2.2.19)

$$\eta(p,m) = 0 \qquad \text{otherwise,}$$

where g is any integer. Except where noted, a quadratic profile is assumed for the remainder of the discussions in this thesis.

Buralli and Morris[17] analyzed the effects of unwanted orders of a diffractive lens on the MTF of the lens. They define an important, and convenient, measure of the efficiency of a diffractive optical element called the *integrated efficiency*. This parameter serves as the limiting value for the MTF, that is, the MTF tends towards the integrated efficiency rather than unity at low spatial frequencies.

In general, diffraction efficiency is a complicated function of zone spacing, incident angle, wavelength, etc. Therefore different *local* efficiencies can exist over the surface of the element. If the pupil function of a diffractive lens is given by

$$P(u,v) = t_{m=1}(u,v)\exp\left[i\frac{k}{n'}W_{m=1}(u,v)\right] + t_{BG}(u,v)\exp\left[i\frac{k}{n'}W_{BG}(u,v)\right], \quad (2.2.20)$$

where $t_{m=1}$ is the transmission function for the first diffracted order, and t_{BG} is the transmission function of other diffracted orders, which give rise to background light, then the local efficiency is given by

$$\eta_{local}(u,v) = \left|t_{m=1}(u,v)\right|^2. \quad (2.2.21)$$

The integrated efficiency defined by Buralli and Morris is the pupil-averaged local efficiency, or

$$\eta_{int} = \frac{1}{A_{pupil}} \int_{-\infty}^{\infty} \int_{-\infty}^{\infty} \eta_{local}(u,v)\,du\,dv, \tag{2.2.22}$$

where A_{pupil} is the area of the exit pupil, and $\eta_{local}(u,v) \equiv 0$ for points outside the pupil.

For polychromatic applications, $\eta_{int,poly}$ is found by integrating over the wavelength band

$$\eta_{int,poly} = \frac{\int_{\lambda\,min}^{\lambda\,max} \eta_{int}(\lambda)\,d\lambda}{\lambda_{max} - \lambda_{min}}, \tag{2.2.23}$$

where $\eta_{int}(\lambda)$ is the pupil-averaged efficiency for each wavelength.

For diffractive lenses where the f/number is greater than 10, the zone spacing can be considered large compared to a wavelength of light, and scalar diffraction theory is valid.[18] In this case the local efficiency is assumed constant over the surface of the lens, and the integrated efficiency is equal to the scalar efficiency. The integrated efficiency is therefore given by Eq. (2.2.16). Integrating Eq. (2.2.16) over the wavelength band yields the following approximate expression for the polychromatic integrated efficiency in the first order, m = 1:

$$\eta_{int,poly} \cong 1 - \frac{\pi^2}{36}\left(\frac{\Delta\lambda}{\lambda_0}\right)^2, \tag{2.2.24}$$

where $\Delta\lambda$ is the wavelength band centered on the design wavelength λ_0. Figure 2.2.4 shows the effect of $\Delta\lambda$ on the integrated efficiency.

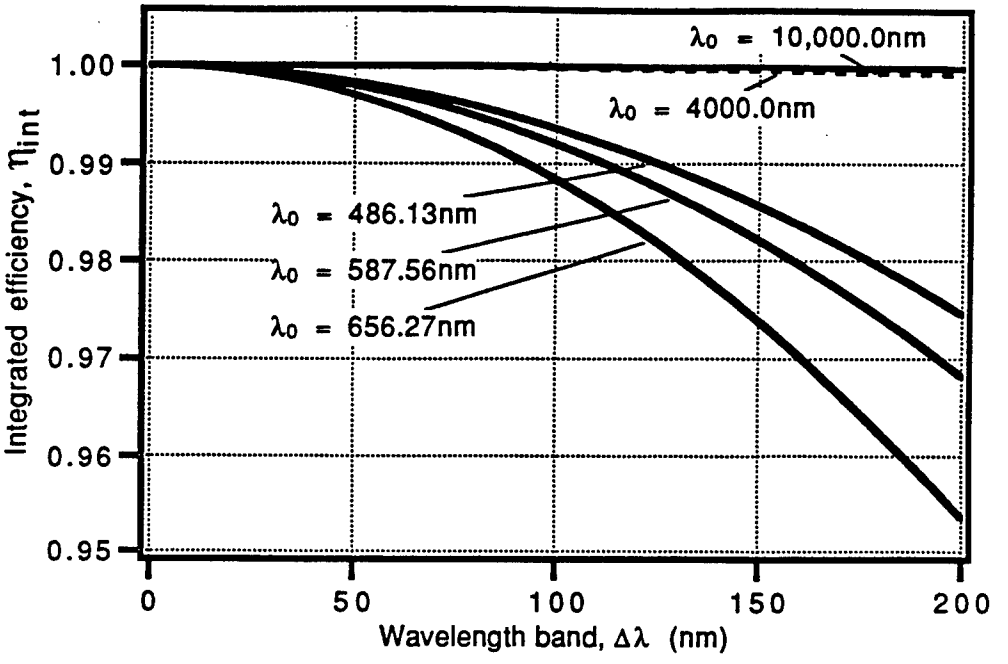

Fig. 2.2.4. The effect of wavelength band on the integrated efficiency. The center wavelengths shown are λ_0 = F, d, and C lines, as well as the center of the 3-5μm and 8-12μm bands.

Show in Fig. 2.2.4 are plots for $\lambda_0 = 0.4861\mu m$ (C line), 0.5876μm (d line), 0.4861μm (F line), 4μm, and 10μm,. As the design wavelength λ_o increases, the effects of the bandwidth $\Delta\lambda$ on the integrated efficiency decreases. In the infrared regions, the wavelength band has a negligible effect on the integrated efficiency.

Buralli and Morris also show that the integrated efficiency is an overall scaling factor for the OTF, that is

$$\mathrm{OTF}(f_x,f_y) \cong \frac{\eta_{int}\int_{-\infty}^{\infty}\int_{-\infty}^{\infty} P_{m=1}(u,v)\otimes P_{m=1}(u,v)\,du\,dv}{\int_{-\infty}^{\infty}\int_{-\infty}^{\infty}|t_{m=1}(u,v)|^2\,du\,dv} + (1-\eta_{int})\delta_{f_x,0}\delta_{f_y,0}, \quad (2.2.25)$$

where $\otimes$ is the autocorrelation, and $\delta_{a,b}$ is the Kronecker delta. From Eq. (2.2.25) we see that the OTF is scaled by η_{int} except at $(f_x,f_y) = (0,0)$ where the OTF = 1. Figure 2.2.5 shows a plot of the MTF of a diffractive lens with $\lambda_0 = 10\mu m$ and $\Delta\lambda = 4\mu m$.

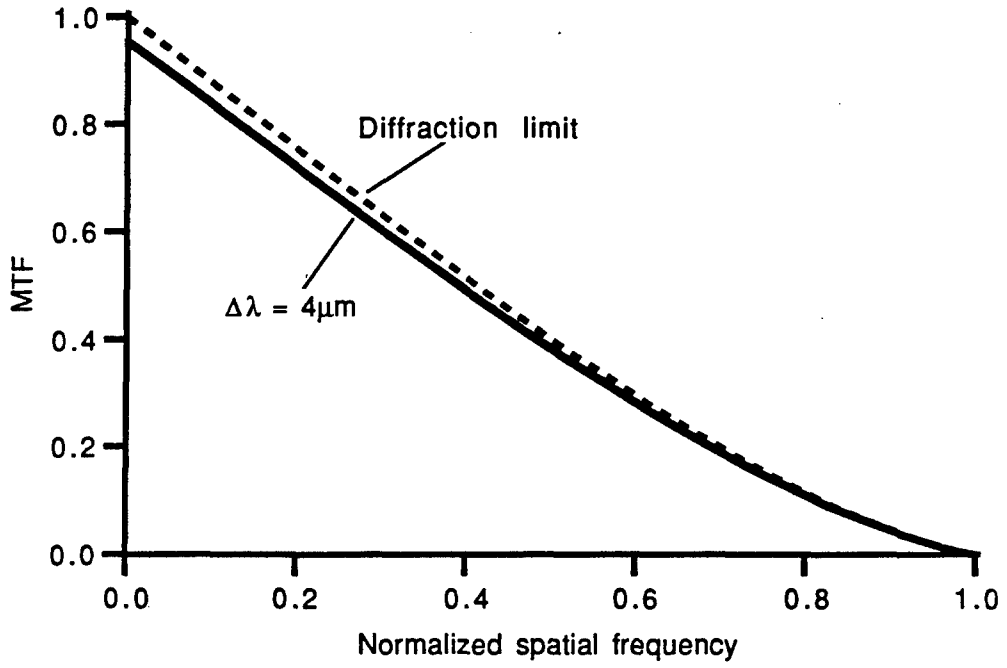

Fig. 2.2.5. MTF of a diffractive lens with $\lambda_0 = 10\mu m$ and a wavelength band $\Delta\lambda = 4\mu m$. The value of $\eta_{int,poly}$ is 0.956.

2.3 Thin lens model

2.3.1. In optical design software

Sweatt[19] and Kleinhans[20] showed that a diffractive lens and a thin lens with an infinite index are mathematically equivalent. When designing diffractive lenses, it is often advantageous to utilize this thin-lens model, however, with lens design programs, an infinite index is not possible. For the majority of applications, however, a value of $n_s(\lambda_o)$=10,001 works well.[21] From Eq. (2.2.13) we see that the power of a diffractive lens is a linear function of wavelength, so the index of refraction, n_s, of the model lens must be scaled accordingly, as in Eq. (2.3.1),

$$n_s(\lambda) = \frac{\lambda}{\lambda_o}\left(n_s(\lambda o) - 1\right) + 1 , \tag{2.3.1}$$

where λ_o is the design wavelength. This equation can in turn be substituted into the familiar Abbe ν-number formula

$$\nu = \frac{n_s(\lambda_m) - 1}{n_s(\lambda_s) - n_s(\lambda_l)}, \tag{2.3.2}$$

where λ_s, λ_m, and λ_l, are the short, middle, and long wavelengths, respectively, to find an expression for the ν number of a diffractive lens. This expression is found to be

$$\upsilon_{dif} = \frac{\lambda_m}{\lambda_s - \lambda_l} . \tag{2.3.3}$$

For visible light, using the F, d, and C lines, the ν number of a diffractive lens is found to be ν_d = -3.45. Since conventional glasses have ν numbers which fall between 20 and 90,

the diffractive lens is much more dispersive than glass and in the opposite direction, indicating that a low-power, positive diffractive lens might be used to achromatize a positive refractive lens.

The surface curvatures of the thin lens model must be chosen to give not only the correct power, but also the proper bending parameter, or shape to the lens. Welford[22] defines the bending parameter, B, as

$$B = \frac{c_1 + c_2}{c_1 - c_2}, \tag{2.3.4}$$

where c_1 and c_2 are the surface curvatures of the thin lens. As n -> ∞, however, c_1 -> c_2 -> c_s, and the bending parameter given by Eq. (2.3.4) becomes indeterminate. Buralli[23] defines a new bending parameter, B', as

$$B' = \frac{B}{n-1} = \frac{c_1 + c_2}{(n-1)(c_1 - c_2)} = \frac{c_1 + c_2}{\phi}, \tag{2.3.5}$$

where ϕ is the power of the lens. As n -> ∞, Eq. (2.3.5) becomes

$$B' = \frac{2c_s}{\phi}, \tag{2.3.6}$$

where c_s is the curvature of the diffractive lens substrate. Equation (2.3.6) remains finite with an infinite index, and is used with the thin lens equation to find the correct surface curvatures of the thin lens model. The results are

$$c_1 = \frac{\phi_o}{2}\left(B' + \frac{1}{n_s - 1}\right) \tag{2.3.7}$$

and

$$c_2 = \frac{\phi_o}{2}\left(B' - \frac{1}{n_s - 1}\right). \qquad (2.3.8)$$

Additionally, if the higher order phase terms in Eq. (2.2.14) are non-zero, one of the surfaces of the lens model must be aspheric. Since the model is assumed to have zero thickness, which surface is aspheric is immaterial. We assume a surface sag of the form

$$z(r) = \frac{cr^2}{1+\sqrt{1-(cr)^2}} + dr^4 + er^6 + fr^8 + gr^{10} \qquad (2.3.9)$$

which can be expanded in a Taylor series (to tenth order) as

$$z(r) = \frac{c}{2}r^2 + \left(\frac{c^3}{8} + d\right)r^4 + \left(\frac{c^5}{16} + e\right)r^6 + \left(\frac{5c^7}{128} + f\right)r^8 + \left(\frac{7c^9}{256} + g\right)r^{10}. \quad (2.3.10).$$

The additional optical path introduced by the surface of the refractive surface described in Eq. (2.3.10) is equal to $-\Delta n\, z(r)$, where $\Delta n = \pm(n_S - 1)$ is the change in refractive index at the surface. The plus or minus sign for Δn depends on whether the aspheric surface is on the front or back surface of the lens. If the phase introduced by the diffractive lens is given by Eq(2.2.14), the additional optical path introduced by a diffractive lens is $(\lambda_o/2\pi)\varphi(r)$, or more explicitly,

$$OPD_{diff} = \frac{\lambda_o}{2\pi}\varphi(r) = \lambda_o\left(Ar^2 + Dr^4 + Er^6 + Fr^8 + Gr^{10}\right). \qquad (2.3.11)$$

By equating terms in Eqs. (2.3.10) and (2.3.11), we see that the aspheric coefficients for the model lens are defined by

$$D = -\frac{\Delta n}{\lambda_o}\left(\frac{c^3}{8} + d\right), \tag{2.3.12a}$$

$$E = -\frac{\Delta n}{\lambda_o}\left(\frac{c^5}{16} + e\right), \tag{2.3.12b}$$

$$F = -\frac{\Delta n}{\lambda_o}\left(\frac{5c^7}{128} + f\right), \tag{2.3.12c}$$

$$G = -\frac{\Delta n}{\lambda_o}\left(\frac{7c^9}{256} + g\right). \tag{2.3.12d}$$

Diffractive lenses are often designed on planer surfaces, to simplify fabrication. In this case, the curvature terms, c^n, in Eqs. (2.3.12) are negligibly small compared with the aspheric coefficients, d, e, f, and g. Equations (2.3.12) provide a convenient way to convert between the phase function and thin lens representations of a diffractive lens, and are especially useful when implemented as a macro in optical system design software. OSLO, for example, provides two Star commands, SWEATT2DFR and DFR2SWEATT, which use the above equations to convert between the Sweatt and phase models of a diffractive surface.

2.3.2. Third order aberrations

A convenient method to derive the third-order aberrations of a diffractive lens is to use the thin-lens model described in section 2.2.2. The third-order aberrations of a diffractive lens can be found by beginning with the third-order aberrations of a thin lens and allowing the index to approach infinity.[13, 19, 20, 23] The third-order wavefront aberration polynomial, W, as a function of normalized object height, h, and normalized polar pupil coordinates ρ and ϕ_p, is[24]

$$W(h,\rho,\cos\phi_p) = \frac{1}{8}S_I\rho^4 + \frac{1}{2}S_{II}h\rho^3\cos\phi_p + \frac{1}{2}S_{III}h^2\rho^2\cos^2\phi_p + \frac{1}{4}(S_{III} + S_{IV})h^2\rho^2 + \frac{1}{2}S_V h^3\rho\cos\phi_p \quad , \tag{2.3.13}$$

where the Seidel sums, S_I-S_V, for a thin lens with the stop in contact are given by

(Spherical aberration)

$$S_I = \frac{y^4\phi^3}{4}\left[\frac{n+2}{n(n-1)^2}B^2 + \frac{4(n+1)}{n(n-1)}BT + \frac{3n+2}{n}T^2 + \left(\frac{n}{n-1}\right)^2\right] + 8Gy^4(\Delta n), \quad (2.3.14a)$$

(Coma)

$$S_{II} = \frac{-y^2\phi^2 H}{2}\left[\frac{n+1}{n(n-1)}B + \frac{2n+1}{n}T\right], \quad (2.3.14b)$$

(Astigmatism)

$$S_{III} = H^2\phi, \quad (2.3.14c)$$

(Petzval curvature)

$$S_{IV} = \frac{H^2\phi}{n}, \quad (2.3.14d)$$

(Distortions)

$$S_V = 0. \quad (2.3.14e)$$

In Eqs. (2.3.14a)–(2.3.14e), n is the refractive index, y is the marginal ray height, ϕ is the power of the lens, $H=-\bar{u}y$ is the Lagrange invariant, G is the fourth-order aspheric coefficient, Δn is the change in refractive index on passing through the lens, B is the bending parameter (Eq. (2.3.4)) and T is the conjugate parameter, defined as

$$T = \frac{u+u'}{u-u'}, \quad (2.3.15)$$

where u and u' are the paraxial ray angles for the marginal ray entering and exiting the thin lens.

To find the Seidel coefficients for a diffractive lens, the limits of the above expressions are taken as $n \to \infty$ and as c_1 and $c_2 \to c_s$; it then becomes necessary to use the bending parameter, B', given in Eq. (2.3.6). Additionally, the S_I term must take into account any additional OPD introduced by the fourth order phase coefficient D. The resulting Seidel sums, for a diffractive lens with stop in contact, are[13]

(Spherical aberration)

$$S_I = \frac{y^4\phi^3}{4}\left[B'^2 + 4B'T + 3T^2 + 1\right] - 8D\lambda m y^4, \tag{2.3.16a}$$

(Coma)

$$S_{II} = \frac{-y^2\phi^2 H}{2}\left[B' + 2T\right], \tag{2.3.16b}$$

(Astigmatism)

$$S_{III} = H^2\phi, \tag{2.3.16c}$$

(Petzval curvature)

$$S_{IV} = 0, \tag{2.3.16d}$$

(Distortion)

$$S_V = 0. \tag{2.3.16e}$$

From Eqs. (2.3.16d) and (2.3.16e) we see that a diffractive lens with stop in contact has no Petzval or distortion. Although a stop shift will not be considered in this thesis, Buralli and Morris[13] show how it can be used to eliminate coma and astigmatism, although it will introduce distortion. In chapter 3, the above equations will be used with Eqs. (2.3.14) to design a hybrid diffractive/refractive achromat with zero spherical or coma. In the design of diffractive lenses, the power ϕ and conjugate parameter T are usually specified, leaving the bending parameter B' and the fourth order phase coefficient D as the remaining degrees of freedom. As will be seen in chapter 3, B' and D, along with the bending parameter of the refractive element, provide enough degrees of freedom to design a cemented hybrid achromat with no spherical or coma.

2.4. Summary of Chapter 2

In this chapter we surveyed some of the basics needed to design diffractive lenses. In section 2.2, the diffractive lens and how it is described mathematically was reviewed. Beginning with full-period Fresnel zones, it was shown that a quadratic phase function could yield 100% scalar efficiency in the first order. In general, however, the efficiency will not be constant across the surface of a diffractive element, nor will it be constant over a bandwidth. In these cases, a useful parameter to use is the *integrated efficiency*. A simple formula was presented for the polychromatic integrated efficiency when the diffractive lens has an f/number greater than about ten. This is almost always the case when the diffractive lens is used for achromatization.

Section 2.3 described how to model a diffractive lens as a very thin lens with an infinite refractive index. The thin lens model is useful when designing diffractive elements on conventional lens design programs. A good approximation to an infinite refractive index in a lens design program is about 10,000 for the design wavelength. A formula was presented for calculating refractive indices at other wavelengths. We then showed how to convert between the phase function representation and the thin lens model, giving formulae for surface curvatures and aspheric coefficients. Finally, the thin lens representation was used to derive the Seidel coefficients for a diffractive lens. The Seidel coefficients for a diffractive lens can be used the same manner as those for refractive lenses when designing achromats.

2.5. References for Chapter 2

1. L. B. Lesem, P. M. Hirsch, J. A. Jordan, "The kinoform: a new wavefront reconstruction device," IBM J. Res. Dev. **13,** 150-155 (1969).
2. J. A. Jordan, P. M. Hirsch, L. B. Lesem, D. L. V. Rooy, "Kinoform lenses," Appl. Opt. **9,** 1883-1887 (1970).
3. W. B. Veldkamp, G. J. Swanson, D. C. Shaver, "High efficiency binary lenses," Opt. Comm. **53,** 353-358 (1985).
4. G. J. Swanson, W. B. Veldkamp, "Binary lenses for use at 10.6 micrometers," Opt. Eng. **24,** 791-795 (1985).
5. G. J. Swanson, W. B. Veldkamp, "Diffractive optical elements for use in infrared systems," Opt. Eng. **28,** 605-608` (1989).
6. K. Miyamoto, "The phase Fresnel lens," J. Opt. Soc. Am. **51,** 17-20 (1961).
7. G. G. Sliusarev, "Optical systems with phase layers," Sov. Phys. Dokl **2,** 161-163 (1957).
8. A. Tudorovskii, "An objective with a phase plate," Opt. and Spect. **2,** 126-133 (1959).
9. T. Stone, N. George, "Hybrid diffractive-refractive lenses and achromats," Appl. Opt. **27,** 2960-2971 (1988).
10. P. Twardowski, P. Meyrueis, "Design of some achromatic imaging hybrid diffractive-refractive lenses," *Holographic Optics III: Principles and Applications*, Proc. SPIE, **1507,** pp. 55-65 (1991).
11. H. Madjidi-Zolbanine, C. Froely, "Holographic correction of both chromatic and spherical aberrations of single glass lenses," Appl. Opt. **18,** 2385-2393 (1979).
12. A. P. Wood, "Using hybrid refractive-diffractive elements in infrared Petzval objectives," Proc. SPIE, **1354**, (1990).

13. D. A. Buralli, G. M. Morris, "Design of a wide field diffractive landscape lens," Appl. Opt. **28,** 3950-3959 (1989).

14. H. Dammann, "Blazed synthetic phase only holograms," Optik **31,** 95-104 (1970).

15. D. A. Buralli, G. M. Morris, J. R. Rogers, "Optical performance of holographic kinoforms," Appl. Opt. **28,** 976-983 (1989).

16. J. W. Goodman, *Introduction to Fourier Optics* (McGraw-Hill, New York, 1968), p. 80.

17. D. Buralli, G. M. Morris, "Effects of diffraction efficiency on the MTF of diffractive lenses," Appl. Opt. (To appear in 1993).

18. J. A. Cox, et al., "Diffraction efficiency of binary optical elements," *Computer and Optically Formed Holographic Optics*, Proc. SPIE, **1211,** pp. 116-123 (1990).

19. W. Sweatt, "Describing holographic optical elements as lenses," J. Opt. Soc. Am. **67,** 803-808 (1977).

20. W. A. Kleinhans, "Aberrations of curved zone plates and Fresnel lenses," Appl. Opt. **16,** 1701-1704 (1977).

21. D. C. Sinclair, "Designing diffractive optics using the Sweatt model," Sinclair Optics Design Notes, Vol. 1, No. 1 (Winter 1990).

22. W. T. Welford, *Aberrations of Optical Systems* (Hilger, Bristol, 1986), p. 227.

23. D. A. Buralli, G. M. Morris, "Design of diffractive singlets for monochromatic imaging," Appl. Opt. **30,** 2151-2158 (1991).

24. Reference 22, pp. 130-140.

3. Diffractive/refractive achromat design

3.1. Introduction

The idea of using a diffractive surface to achromatize a refractive lens is not new. Sliusarev,[1] Tudorovskii,[2] and Miyamoto[3] discussed the idea that a "phase plate" or a "phase Fresnel lens" might be used to correct longitudinal aberration. Madjidi-Zolbanine,[4] Stone and George,[5] Faklis and Morris,[6] and Twardowski and Meyrueis[7] discuss achromatization with holographic lenses. This chapter discusses the use of rotationally symmetric, surface-relief diffractive lenses in achromatization. The approach we will take is the traditional approach to designing an achromatic doublet.

The design method for an achromatic doublet is well known.[8, 9, 10] If the doublet is not to be cemented, then there are enough degrees of freedom to correct both spherical and coma. With careful choice of glasses, however, a cemented doublet with no, or very little, spherical and coma can be designed. For the treatment in this chapter, we will consider only a positive doublet made of thin lenses with the main focusing elements in front, as in Fig. 3.1.1.

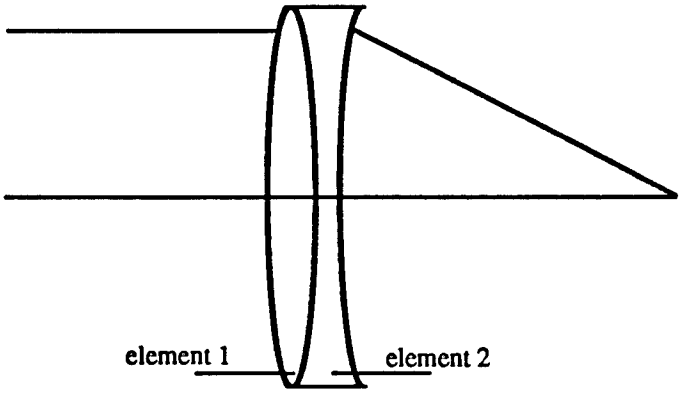

Fig 3.1.1 Schematic of an achromatic doublet.

Aberrations manifest themselves as phase errors in an optical system. Using equations presented in Section 3.2, the effects of third-order aberrations on the point spread function (PSF) and modulation transfer function (MTF) of a doublet are discussed.

Section 3.2 uses a wave propagation approach to discuss how decentering or tilting one of the elements with respect to the other affects the doublet's PSF and MTF. Section 3.3 provides two examples of how achromats are designed using equations described in the previous chapter. First a conventional achromat with minimal spherical and coma is designed, and then the method is extended to design a hybrid diffractive/refractive achromat.

3.2. Effects of aberrations on PSF and MTF

3.2.1. Third order aberrations

The point spread function of an optical system is defined as the modulous-squared Fourier transform of the system pupil function:[11]

$$PSF(x,y) = \left| \int\int_{-\infty}^{\infty} P(\xi,\eta) \exp\left[-i \frac{2\pi}{\lambda f} (x\xi + y\eta) \right] d\xi\, d\eta \right|^2 \tag{3.2.1}$$

where $P(\xi,\eta)$ is the pupil function and x and y are image plane coordinates. Constants, which serve only scale the PSF, have been dropped from Eq. (3.2.1). The modulation transfer function can be defined as the modulous of the Fourier transform of the PSF:[12]

$$MTF(f_x, f_y) = \frac{\left| \int\int_{-\infty}^{\infty} PSF(x,y) \exp\left[-i2\pi (x f_x + y f_y) \right] dx\, dy \right|}{\left| \int\int_{-\infty}^{\infty} PSF(x,y)\, dx\, dy \right|}. \tag{3.2.2}$$

The wavefront aberration $W(h,\rho,\cos\phi_p)$ defined by Eq. (2.3.13) introduces a phase modulation across the pupil in a manner described by,

$$P(\xi,\eta) = A(\xi,\eta) \exp\left[ikW(h,\xi,\eta) \right], \tag{3.2.3}$$

where $A(\xi,\eta)$ is unity for points inside the aperture and zero for points outside the aperture, $k = 2\pi/\lambda$, and $W(h,\xi,\eta)$ is given by Eq. (2.3.13) with the change of variables $\xi = \rho \sin\phi$, and $\eta = \rho \cos\phi$. From Eq. (3.2.3) it is seen that aberrations introduce phase distortions in the pupil, and in general this will lower the contrast in the image.[13] One important point should be made regarding Eq. (3.2.3). There is a field dependence, h, in W which does not appear in P. This is because the Fourier transforming property of a lens is based on a spatially invariant system. A system with aberrations is not spatially

invariant. Therefore, the PSF can be found at only one object point at a time. There is little more that can be said about the effects of aberrations on the PSF and MTF of a lens– Eqs. (3.2.1) and (3.2.2) are so complicated that PSF and MTF calculations are always carried out numerically.

As an example, we will look at the PSF and MTF of an f/5, 50mm focal length, planer diffractive lens, paraxial zone spacing, 10° half field of view, and an infinitely distant object. The Seidel coefficients can be calculated using Eqs. (2.3.16). The resulting values are

$$S_I = 8.510\lambda \tag{3.2.4a}$$

$$S_{II} = -15.005\lambda \tag{3.2.4b}$$

$$S_{III} = 26.458\lambda \tag{3.2.4c}$$

$$S_{IV} = S_V = 0.0 \tag{3.2.4d}$$

The PSF's for the on axis (h=0) and full field (h=1) cases, at the paraxial image plane, are shown in Fig 3.2.1.

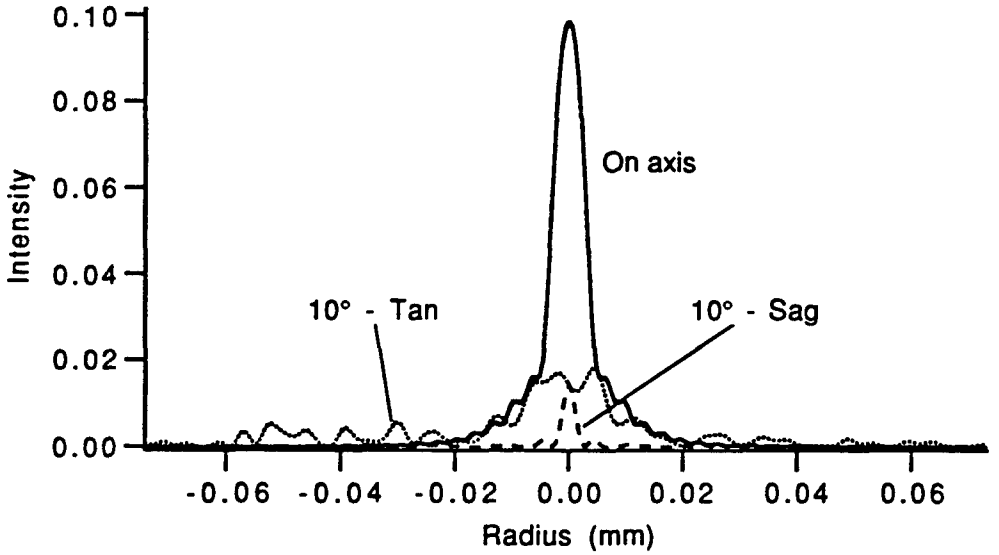

Fig. 3.2.1 Point spread functions for an f/5, 50mm focal length, planer diffractive lens with paraxial zone spacing. The half field of view is 10°, and the object is at infinity. The plot has been normalized so that the peak value for an unaberrated wavefront is 1.0.

The reference wavelength for Fig. 3.2.1 plot was chosen to be the d-line ($\lambda_0 = 0.58756\mu m$). The data was normalized so that the peak value for an unaberrated wavefront is 1.0. The MTF of the same lens can be found with Eq. (3.2.2). The results are shown in Fig. 3.2.2.

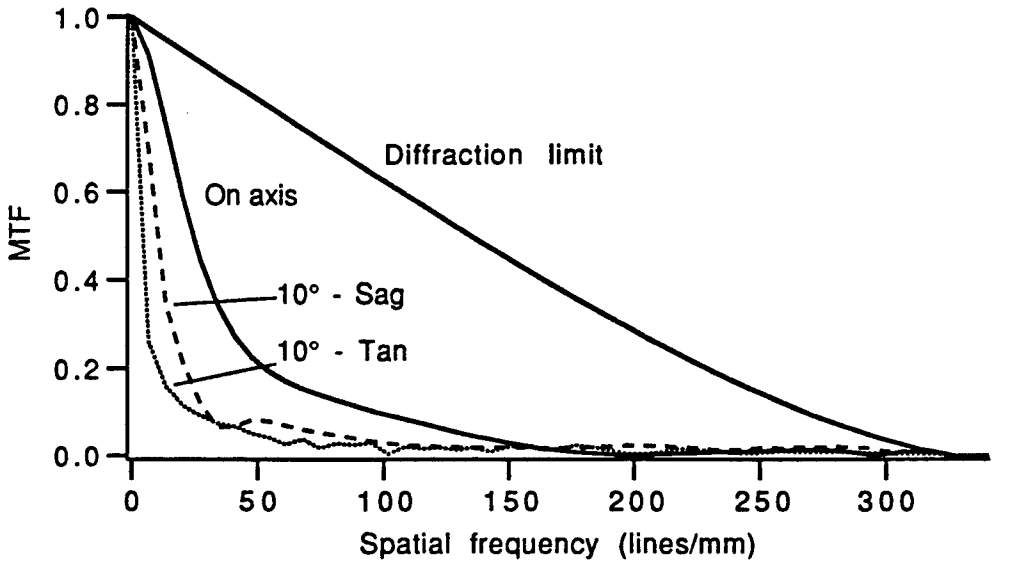

Fig. 3.2.2 Modulation transfer functions for the lens described above.

As expected, the aberrations cause a reduction in the peak value of the PSF and a decrease in the resolution, or MTF of the lens as well.

For an achromat, where there are two elements with different transfer functions, we take pupil function to be the product of the pupil functions of the individual elements, P_1 and P_2. The pupil function of the n^{th} element is given by

$$P_n(\xi,\eta) = A_n(\xi,\eta)\exp\{ik\,W_n(h,\xi,\eta)\}, \tag{3.2.5}$$

where A_n is the aperture function, and W_n is the wavefront error. The two element system shown schematically in Fig. 3.2.3.

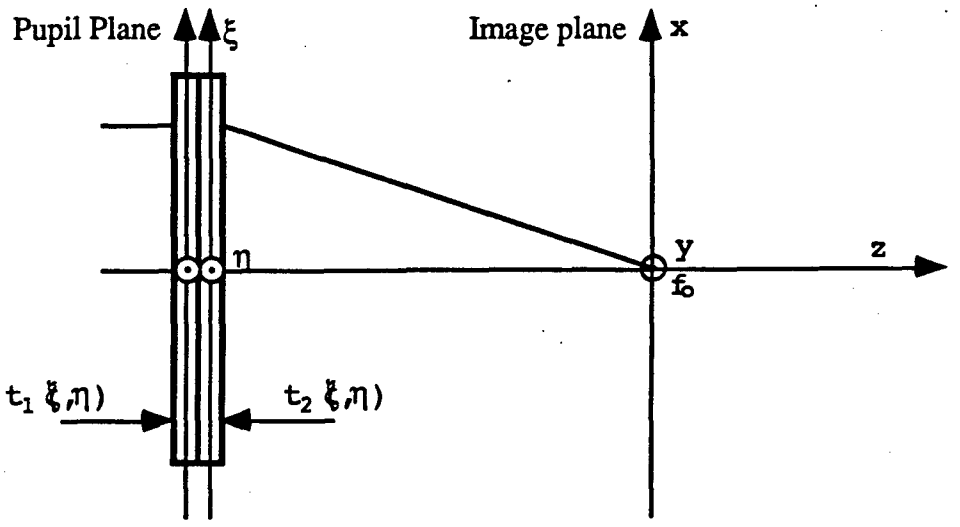

Fig. 3.2.3 Schematic of achromatic lens. The two transfer functions $t_1(\xi,\eta)$ and $t_2(\xi,\eta)$ are taken to have zero space between them.

In Fig. 3.2.3, the transfer functions, $t_n(\xi,\eta)$, of the n^{th} element are given by

$$t_n(\xi,\eta) = P_n(\xi,\eta)\exp(ikn_n\Delta_n)\exp\left[-\frac{ik}{2f_n}\left(\xi^2+\eta^2\right)\right] \tag{3.2.6}$$

where f_n and Δ_n are the focal length and thickness of the n^{th} element, respectively. We will assume thin lenses, with no space between the transmission functions of the first and second elements. The PSF of this system can be expressed as

$$PSF(x,y) =$$

$$\left|\int\int_{-\infty}^{\infty} A_1(\xi,\eta)A_2(\xi,\eta)\exp\left[-i\frac{2\pi}{\lambda f}(x\xi+y\eta)+ik\left(W_1(h,\xi,\eta)+W_2(h,\xi,\eta)\right)\right]d\xi\,d\eta\right|^2, \tag{3.2.7}$$

and the MTF is again given by Eq. (3.2.2). As seen in Eq. (3.2.7), the aberrations of one element of the achromat can be used to compensate for aberrations in the other element by choosing $W_2(h,\xi,\eta) = -W_1(h,\xi,\eta)$. The achromats designed in sections 3.3.1 and 3.3.2

provide examples of how spherical and coma can be eliminated by balancing the aberrations in each element against each other.

3.2.2. Decenter and Tilt

In addition to the third-order aberrations, doublets can also be affected by fabrication errors such as decenter and tilt, shown schematically in Figs. 3.2.4 and 3.2.5.

For the case of decenter, the elements of the doublet have transmission functions given by

$$t_1(\xi,\eta) = P_1(\xi,\eta)\exp(ikn_1\Delta_1)\exp\left[-\frac{ik}{2f_1}(\xi^2+\eta^2)\right], \tag{3.2.8}$$

and

$$t_2(\xi,\eta) = P_2(\xi+\Delta\xi,\eta+\Delta\eta)\exp(ikn_2\Delta_2)\exp\left[-\frac{ik}{2f_2}\left((\xi+\Delta\xi)^2+(\eta+\Delta\eta)^2\right)\right], \tag{3.2.9}$$

where P_n is given by Eq. (3.2.5), and $\Delta\xi$ and $\Delta\eta$ are the shift of the second element with respect to the first in the ξ and η directions, respectively. The incident field, $U_0(\xi,\eta)$, is taken to be a plane wave, ie. $U_0(\xi,\eta) = 1$. The field leaving the second element is given by

$$U_2(\xi,\eta) = U_0(\xi,\eta)t_1(\xi,\eta)t_2(\xi,\eta). \tag{3.2.10}$$

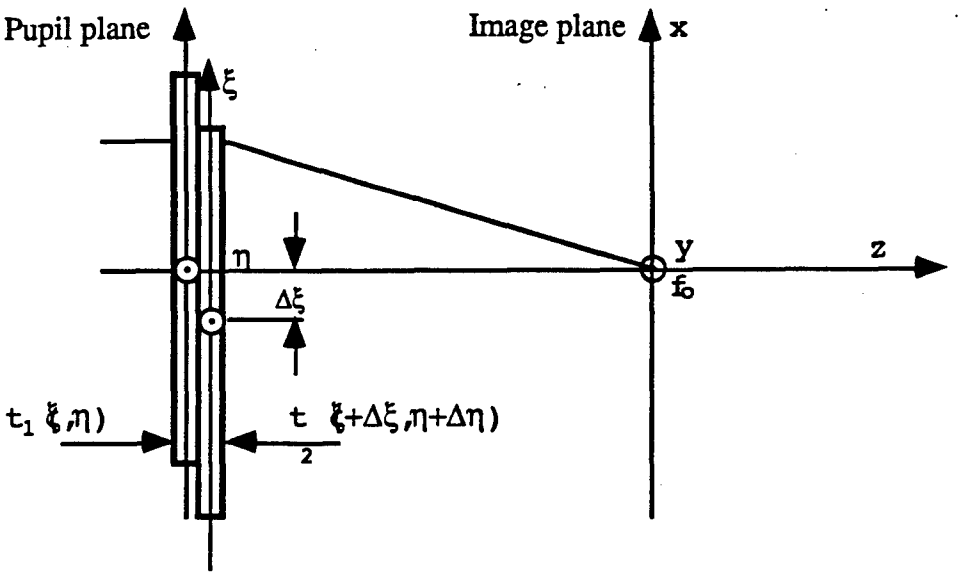

Fig. 3.2.4 Schematic diagram of two decentered transmission functions. The amount of decenter in the ξ axis is given by $\Delta\xi$; decenter in the η axis is given by $\Delta\eta$ (not shown above). The image plane is the paraxial image plane with $\Delta\xi = \Delta\eta = 0.0$.

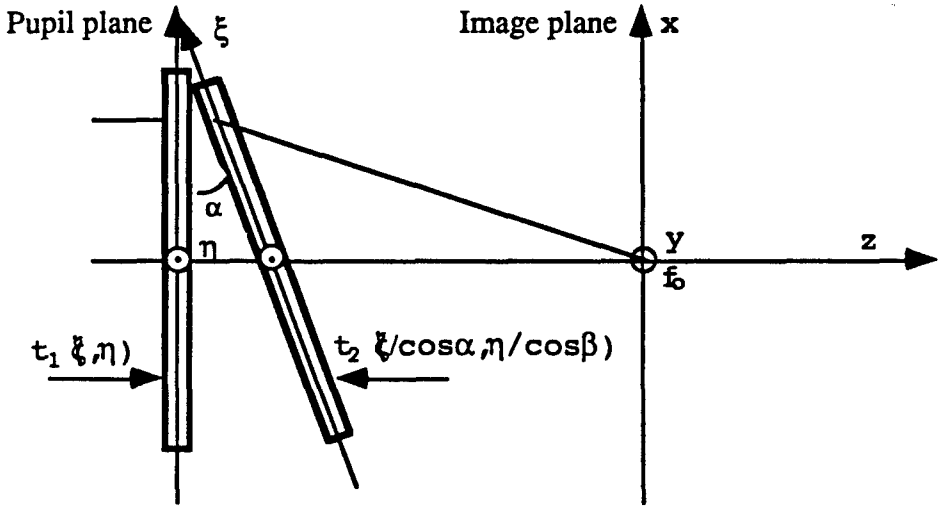

Fig. 3.2.5 Schematic diagram of two transmission functions with tilt or "wedge" between them. The magnitude of wedge in the ξ axis is given by the angle α; tilt in the η axis is given by β (not shown above). The image plane is the paraxial plane with $\alpha = \beta = 0.0$.

A Fresnel propagation yields the following field distribution in the paraxial image plane:

$$U_i(x,y) = \int\int_{-\infty}^{\infty} P_1(\xi,\eta)P_2(\xi+\Delta\xi,\eta+\Delta\eta)\times$$
$$\exp\left[-ik\left(\frac{1}{2f_1}(\xi^2+\eta^2)+\frac{1}{2f_2}(\xi+\Delta\xi)^2+\frac{1}{2f_2}(\eta+\Delta\eta)^2\right)\right]\times$$
$$\exp\left[\frac{ik}{2F}(\xi^2+\eta^2)\right]\exp\left[-\frac{ik}{F}(\xi x+\eta y)\right]d\xi\,d\eta \quad . \qquad (3.2.11)$$

where F is the focal length of the doublet. Terms involving the thicknesses of the elements in Eq. (3.2.11) have been ignored since they can be carried outside the integration, and will disappear when the intensity is found.

Since we are working with thin lenses, the relationship

$$\frac{1}{f_1}+\frac{1}{f_2}=\frac{1}{F}, \qquad (3.2.12)$$

is valid, and Eq. (3.2.11) can be simplified to yield the following:

$$U_i(x,y) = \int\int_{-\infty}^{\infty} P_1(\xi,\eta)P_2(\xi+\Delta\xi,\eta+\Delta\eta)\times$$
$$\exp\left[-\frac{ik}{2f_2}(2\xi\Delta\xi+\Delta\xi^2+2\eta\Delta\eta+\Delta\eta^2)\right]\exp\left[-\frac{ik}{F}(\xi x+\eta y)\right]d\xi\,d\eta \quad . \qquad (3.2.13)$$

The $\Delta\xi^2$ and $\Delta\eta^2$ terms can be carried outside the integral and will have no effect on the functional form. Neglecting these terms, Eq. (3.2.13) now takes the form

$$U_i(x,y) = \int\int_{-\infty}^{\infty} P_1(\xi,\eta)P_2(\xi+\Delta\xi,\eta+\Delta\eta)$$
$$\exp\left[-ik\left(\xi\left(\frac{\Delta\xi}{f_2}+\frac{x}{F}\right)+\eta\left(\frac{\Delta\eta}{f_2}+\frac{y}{F}\right)\right)\right]\exp\left[-\frac{ik}{F}(\xi x+\eta y)\right]d\xi\,d\eta, \qquad (3.2.14)$$

which is simply the Fourier transform of the product P_1P_2 with the frequency variables

$$f_\xi = \frac{1}{\lambda}\left(\frac{\Delta\xi}{f_2}+\frac{x}{F}\right), \quad \text{and} \quad f_\eta = \frac{1}{\lambda}\left(\frac{\Delta\eta}{f_2}+\frac{y}{F}\right). \qquad (3.2.15)$$

If the second element of a doublet is tilted with respect to the first, the transmission functions become

$$t_1(\xi,\eta) = P_1(\xi,\eta)\exp(ikn_1\Delta_1)\exp\left[-\frac{ik}{2f_1}(\xi^2+\eta^2)\right], \qquad (3.2.16)$$

and

$$t_2(\xi,\eta) = P_2\left(\frac{\xi}{\cos\alpha},\frac{\eta}{\cos\beta}\right)\exp(ikn_2\Delta_2)\exp\left[-\frac{ik}{2f_2}\left(\left(\frac{\xi}{\cos\alpha}\right)^2+\left(\frac{\eta}{\cos\beta}\right)^2\right)\right], \qquad (3.2.17)$$

where α and β are tilts about the η and ξ axis, respectively, as in Fig. 3.2.5.

Tilting one lens with respect to the other also introduces a phase error due to the space between two. Since the two lenses are so close together, the field incident on the second lens will be the geometric projection of the first, multiplied by a linear phase term. The transfer function of this wedge is given by

$$t_{wedge}(\xi,\eta) = \exp\left[-ikn_w(\xi\tan\alpha+\eta\tan\beta)\right], \qquad (3.2.18)$$

where n is the index of the material in between the lenses. If the field incident on the first lens is given by U_0, then the field leaving the second lens is

$$U_2(\xi,\eta) = U_0(\xi,\eta)t_1(\xi,\eta)t_{wedge}(\xi,\eta)t_2(\xi,\eta). \tag{3.2.19}$$

We will consider angles which are less than 0.25°. This is within the capabilities of modern technology, and it will also make the mathematics involved much easier. If the angle $\alpha \le 0.25°$, then $\cos(\alpha) \ge 0.99990$. Taking $\cos(\alpha) = \cos(\beta) = 1$, Fresnel propagating to the paraxial image plane and simplifying yields

$$U_i(x,y) = \int\int_{-\infty}^{\infty} P_1(\xi,\eta)P_2(\xi+\Delta\xi,\eta+\Delta\eta)$$
$$\exp\left[-ik\left(\xi\left(\tan\alpha+\frac{x}{F}\right)+\eta\left(\tan\beta+\frac{y}{F}\right)\right)\right]\exp\left[-\frac{ik}{F}(\xi x+\eta y)\right]d\xi\,d\eta, \tag{3.2.20}$$

where again, coefficients outside the integral which only serve to scale the PSF have been dropped. The field at the image plane is found to be the Fourier transform of the product P_1P_2, but with the frequency variables

$$f_\xi = \frac{1}{\lambda}\left(\tan\alpha+\frac{x}{F}\right) \quad \text{and} \quad f_\eta = \frac{1}{\lambda}\left(\tan\beta+\frac{y}{F}\right). \tag{3.2.21}$$

It is trivial to show that if decenter and tilt are combined, the point spread function is given by

$$PSF(x,y) = \left|F.T.\left\{P_1(\xi,\eta)\times P_2(\xi,\eta)\right\}\right|^2, \tag{3.2.22}$$

where F.T.{ } means the Fourier transform whose frequency variables are given by

$$f_\xi = \frac{1}{\lambda}\left(\frac{\Delta\xi}{f_2}+\tan\alpha+\frac{x}{F}\right) \quad \text{and} \quad f_\eta = \frac{1}{\lambda}\left(\frac{\Delta\eta}{f_2}+\tan\beta+\frac{y}{F}\right). \tag{3.2.23}$$

The two pupil functions P_1 and P_2 in Eq. (3.2.22) must be redefined. P_1 can be defined just as in Eq. (3.2.5), that is,

$$P_1(\xi,\eta) = A_1(\xi,\eta)\exp\left[ikW_1(h_1,\xi,\eta)\right]. \tag{3.2.24}$$

Taking into account the effects of decenter and tilt, the pupil function of the second element of the doublet P_2 is given by

$$P_2(\xi,\eta) = A_2(\xi+\Delta\xi,\eta+\Delta\eta)\exp\left[ikW_2(h_2,\xi+\Delta\xi,\eta+\Delta\eta)\right], \tag{3.2.25}$$

where, if θ is the half field of view, h_2 is given by

$$h_2 = \frac{\arctan\left[\sqrt{\tan^2(\alpha+h_1\theta)+\tan^2(\beta)}\right]}{\theta}. \tag{3.2.26}$$

Equation (3.2.26) is derived by calculating what additional field angle is introduced by the tilt angles α and β, given the existing field angle $h_1\theta$.

Substituting Eqs. (3.2.24) and (3.2.25), into Eq. (3.2.22) we find the following expression for the PSF of a doublet:

$$PSF(x,y) = \left|\begin{array}{l} F.T.\{A_1(\xi,\eta)A_2(\xi+\Delta\xi,\eta+\Delta\eta)\times \\ \qquad \exp\left[ik\left(W_1(h_1,\xi,\eta)+W_2(h_2,\xi+\Delta\xi,\eta+\Delta\eta)\right)\right]\} \end{array}\right|^2. \tag{3.2.27}$$

From Eq. (3.2.27) we see that aberrations in each element of a doublet no longer cancel if one of the elements is decentered or tilted with respect to the other. For this reason, it is advantageous to correct aberrations as closely as possible to their origins.

3.3. Thin lens examples

3.3.1. Conventional achromat

In the method described below, we begin with Eqs. (2.3.14a) and (2.3.14b). To make the design process easier, we write these equations, without any aspherics, as

(Spherical aberration)

$$S_{Ij} = \frac{y_j^4 \phi_j^3}{4}\left[a_j B_j^2 + b_j B_j T_j + c_j T_j^2 + d_j\right] \tag{3.3.1}$$

(Coma)

$$S_{IIj} = -\frac{y_j^2 \phi_j^2 H}{2}\left[e_j B_j + f_j T_j\right] \tag{3.3.2}$$

where the coefficients a-e are defined by

$$a_j = \frac{n_j + 2}{n_j (n_j - 1)^2}, \quad b_j = \frac{4(n_j + 1)}{n_j (n_j - 1)}, \quad c_j = \frac{3n_j + 2}{n_j},$$

$$d_j = \left(\frac{n_j}{n_j - 1}\right)^2, \quad e_j = \frac{n_j + 1}{n_j (n_j - 1)}, \quad f_j = \frac{2n_j + 1}{n_j}, \tag{3.3.3}$$

where the subscript j denotes which element of the doublet the parameter belongs to, see Fig. 3.1.1.

If Φ is the desired power of the achromat, and ν_1 and ν_2 are the dispersions of the two elements, then the constraints for an achromat formed by two thin lenses in contact are given by

(Correct total power)

$$\phi_1 + \phi_2 = \Phi, \tag{3.3.4}$$

(Achromatic condition)

$$\frac{\phi_1}{\nu_1} + \frac{\phi_2}{\nu_2} = 0, \tag{3.3.5}$$

(No spherical)

$$S_{I1} + S_{I2} = 0, \tag{3.3.6}$$

(No coma)

$$S_{II1} + S_{II2} = 0, \tag{3.3.7}$$

(Cemented constraint)

$$C_{12} = C_{21} = \frac{\phi_1}{2(n_1 - 1)}(B_1 - 1) = \frac{\phi_2}{2(n_2 - 1)}(B_2 + 1), \tag{3.3.8}$$

where C_{12} is the second surface of the first element and C_{21} is the first surface of the second element.

Combining Eqs. (3.3.4) and (3.3.5) yields the following expression for the power in each element

$$\phi_1 = \frac{\nu_1}{\nu_1 - \nu_2}\Phi \quad \text{and} \quad \phi_2 = \frac{\nu_2}{\nu_2 - \nu_1}\Phi. \tag{3.3.9}$$

For two thin lenses in contact, the height of the marginal ray is equal for both lenses, $y_1 = y_2 = y$, and substituting Eq. (3.3.1) into Eq. (3.3.6) and simplifying yields

$$\phi_1^3\left[a_1B_1^2 + b_1B_1T_1 + c_1T_1^2 + d_1\right] + \phi_2^3\left[a_2B_2^2 + b_2B_2T_2 + c_2T_2^2 + d_2\right] = 0. \tag{3.3.10}$$

The powers of the elements, ϕ_1 and ϕ_2, are given by Eq. (3.3.9) and once the glasses are selected, a_j - e_j are known as well. From the conjugate, T, of the lens as a whole, we can find the individual element conjugates from the following expressions

$$T_1 = \frac{\Phi}{\phi_1}(T + 1) - 1 \quad \text{and} \quad T_2 = \frac{\Phi}{\varphi_2}(T - 1) + 1. \tag{3.3.11}$$

The remaining degrees of freedom in Eq. (3.3.10) are the bending parameters B_1 and B_2. Solving for B_2 yields the following expression

$$\phi_2^3a_2B_2^2 + \phi_2^3b_2T_2B_2 + \phi_2^3\left(c_2T_2^2 + d_2\right) + \phi_1^3\left[a_1B_1^2 + b_1B_1T_1 + c_1T_1^2 + d_1\right] = 0, \tag{3.3.12}$$

which is now in the form

$$\alpha B_2^2 + \beta B_2 + \gamma = 0 \tag{3.3.13}$$

and can be solved with the quadratic equation. Note that the B_1 dependence is buried in the parameter γ. An example of B_2 as a function of B_1, defined by Eq. (3.3.13), is plotted in Fig. 3.3.1. The doublet is an f/4 achromat with BK7 for element 1, F8 for element 2, and a focal length of 100mm.

Equations (3.3.7) and (3.3.2) can be used in a similar fashion to find the proper bending parameters which result in no coma for the doublet. Following the same procedure as above and solving for B_2 results in the expression:

$$B_2 = -\frac{\phi_1^2(e_1 B_1 + f_1 T_1) + \phi_2^2 f_2 T_2}{\phi_2^3 e_2}. \tag{3.3.14}$$

Equation (3.3.14) is also plotted in Fig. 3.3.1

Solving Eq. (3.3.8) for B_2 yields the following relationship

$$B_2 = \frac{\phi_1}{\phi_2}\frac{(n_2 - 1)}{(n_1 - 1)}(B_1 - 1) - 1, \tag{3.3.15}$$

which is plotted in Fig. 3.3.1 as well.

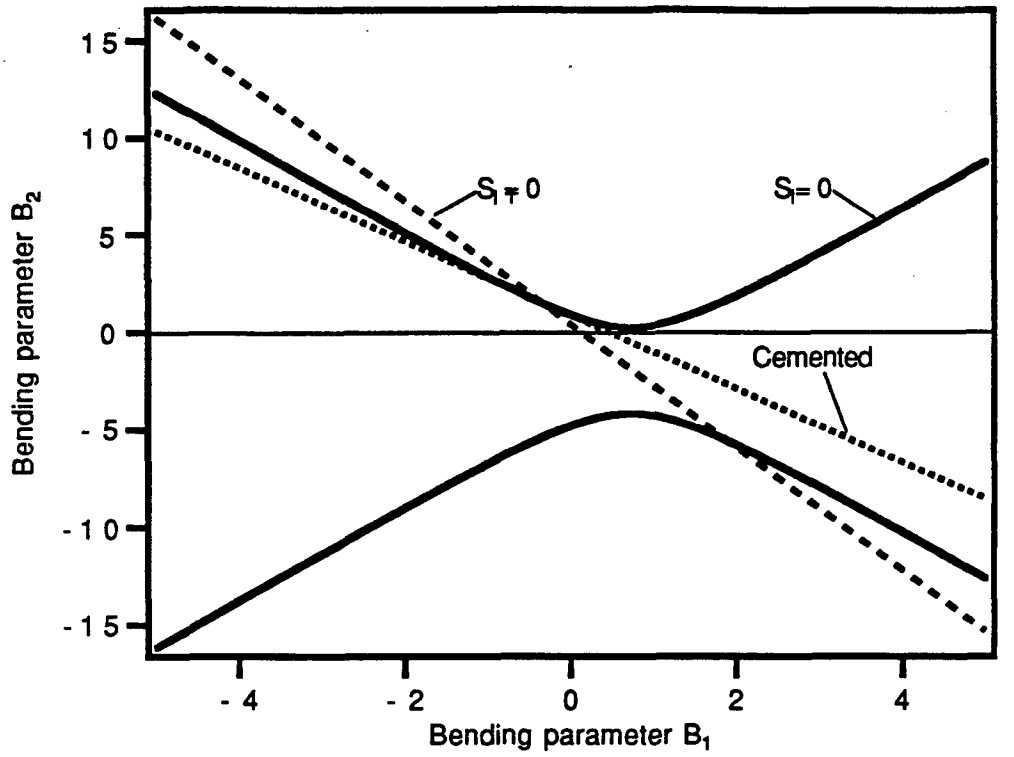

Fig. 3.3.1 The loci of bending parameters where there is no spherical or coma, and where the cemented condition is satisfied. There is no guarantee that all the plots will cross at one point.

From Fig. 3.3.1 we see that there are two combinations of bending parameters where there is no spherical or coma. With a different choice of glass, however, there is no guarantee that even one will exist. The same can be said for satisfying the cemented condition. With this choice of glass, there is one cemented doublet which has no spherical or coma. From the expanded view in Fig. Fig. 3.3.2 we see that the correct bending parameters are B_1 =-0.35 and B_2 = 1.55.

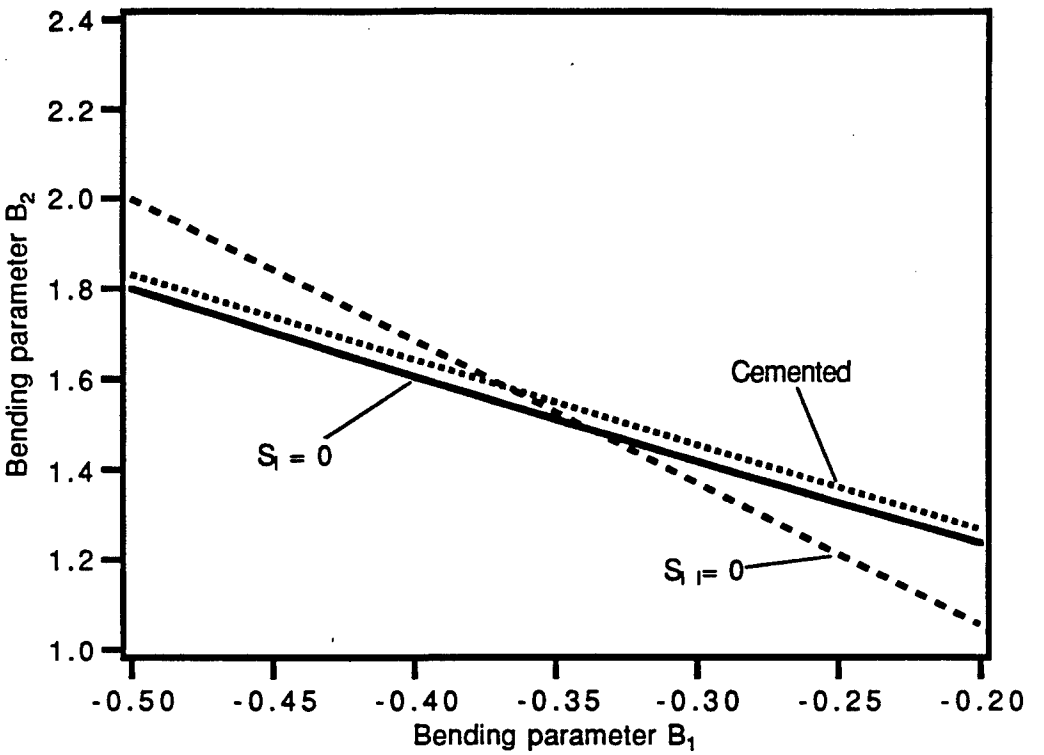

Fig. 3.3.2 Close-up of cemented doublet solution for no spherical or coma.

Equations (3.3.9) and (2.3.4) can be used to find the curvatures of the first and second element. The results are

$$C_{11} = 0.01616\text{mm}^{-1}, \tag{3.3.16a}$$

$$C_{12} = -0.03357\text{mm}^{-1}, \tag{3.3.16b}$$

$$C_{21} = -0.03361\text{mm}^{-1}, \tag{3.3.16c}$$

$$C_{22} = -0.00725\text{mm}^{-1}, \tag{3.3.16d}$$

where C_{11} and C_{12} are the first and second curvatures of first element, and C_{21} and C_{22} are the first and second curvatures of the second element, respectively. These values result in -0.23λ of spherical aberration, and 0.01λ of coma. The curvatures given above provide a good starting point for the final design, to be completed with the help of a lens design program.

3.3.2. Hybrid achromat

A diffractive/refractive hybrid achromat can be designed with the same process as above with only a few modifications. The bending parameter $B_2 = B'$ for the diffractive lens is defined by Eq. (2.3.6), and the Seidel coefficients for spherical and coma are defined by Eqs. (2.3.16a) and (2.3.16b). At first we will neglect the higher order phase term.

Analogous to Eq. (3.3.12), the expression for no spherical aberration in a hybrid lens is

$$\phi_2^3 B_2^2 + \phi_2^3 4T_2 B_2 + \phi_2^3\left(3T_2^2 + 1\right) + \phi_1^3\left[a_1 B_1^2 + b_1 B_1 T_1 + c_1 T_1^2 + d_1\right] = 0. \qquad (3.3.17)$$

Because $\nu = -3.45$ for a diffractive lens, the power in both elements of a hybrid achromat will be positive, according to Eq. (3.3.9). Additionally, the power in the diffractive element will be extremely low. For these reasons, solving Eq. (3.3.17) using a BK7 for the refracting element will produce imaginary numbers for B_1. In fact, the same is true no matter what glass is chosen. At infinite conjugates, therefore, a paraxial diffractive element cannot correct the spherical aberration produced by the refractive element of a hybrid achromat.

To correct this problem, one surface of the glass element can be aspheric, and used to correct the spherical aberration in both lenses. This makes the refractive element significantly more complex, since aspheric surfaces are more difficult to fabricate. This option is attractive, however, because as seen in Eq. (3.2.27), if each element corrects its own aberrations, it eases the tolerances on decentering and tilt.

Another method to correct spherical aberration, equivalent to using an asphere, is to use the fourth order phase coefficient, D, in the diffractive surface. The value of D can be found quite easily by equating Eqs. (2.3.14a) and (2.3.16a). Of course, both bending parameters remain as free variables, but if we look at only the cemented achromat

solutions, then B_2 is determined by B_1. With B_2 defined by Eq. (2.3.6), the cemented requirement becomes

$$C_{12} = C_s = \frac{\phi_1}{2(n_1 - 1)}(B_1 - 1) = \frac{B_2\phi_2}{2}, \tag{3.3.18}$$

where C_{12} is the second surface of the refracting element, and C_s is the curvature of the diffractive lens substrate. Solving Eq. (3.3.18) for B_2 yields the expression

$$B_2 = \frac{\phi_1}{\phi_2}\frac{(B_1 - 1)}{(n_1 - 1)}, \tag{3.3.19}$$

This expression can be used to find D. The net result is

$$D = \frac{\phi_1^3\left[a_1B_1^2 + b_1B_1T_1 + c_1T_1^2 + d_1\right] + \phi_2^3\left[\frac{\phi_1^2}{\phi_2^2}\frac{(B_1 - 1)^2}{(n_1 - 1)^2} + 4\frac{\phi_1}{\phi_2}\frac{(B_1 - 1)}{(n_1 - 1)}T_2 + 3T_2^2 + 1\right]}{32\lambda_0}. \tag{3.3.20}$$

Unlike spherical aberration, real solutions exist for the coma and cemented requirement. The equation defining the solutions for no coma is

$$B_2 = -\frac{\phi_1^2(e_1B_1 + f_1T_1) + \phi_2^2 2T_2}{\phi_2^3}, \tag{3.3.21}$$

and the requirement for a cemented doublet is given by Eq. (3.3.19).

Plots of Eqs. (3.3.19), (3.3.20), and (3.3.21), are shown in Fig. 3.3.3. As seen on the graph, a solution exists at B_1=0.90, B_2=-3.6 and D=-0.417x10^{-3}mm^{-4}.

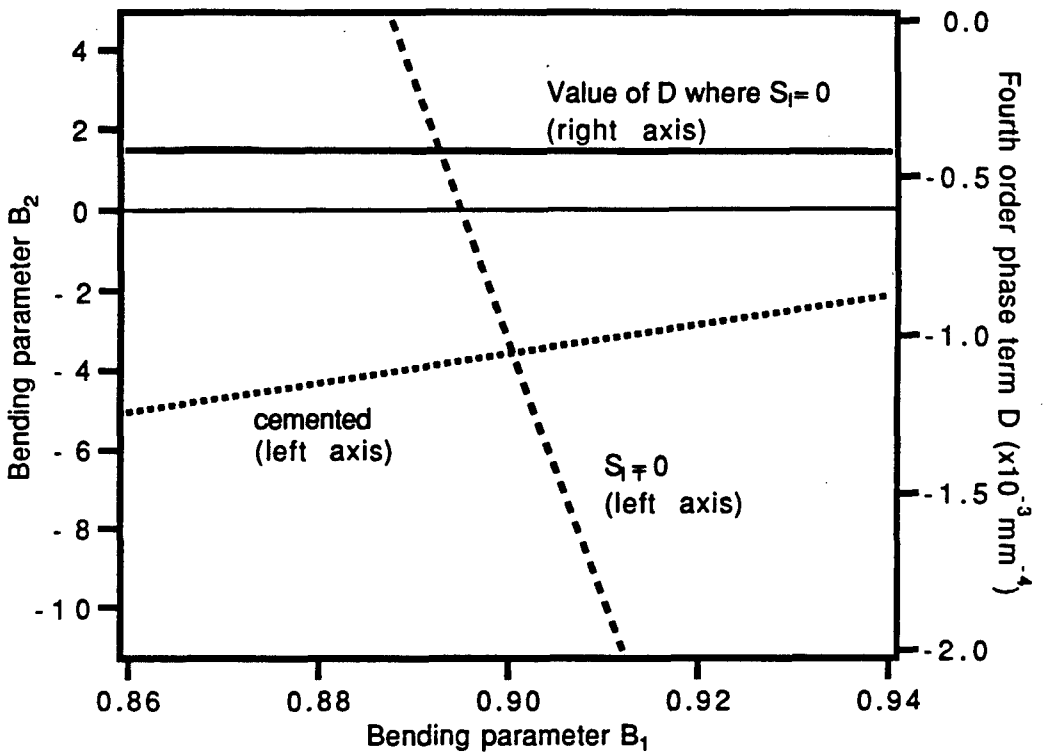

Fig. 3.3.3 Plot showing solution for a cemented hybrid achromat where $S_{II}=0$. Also shown is the value of D, fourth order phase coefficient for the diffractive surface, which is needed to correct spherical aberration.

Equations (3.3.9) and (2.3.4) can again be used to find the curvatures for the BK7 element, and Eqs. (2.2.16) and (2.3.6) can be used to find the second-order phase coefficient, A, and the substrate curvature, C_S, respectively. The results are

$$C_{11} = 0.01744\text{mm}^{-1}, \tag{3.3.22a}$$

$$C_{12} = -0.00092\text{mm}^{-1}, \tag{3.3.22b}$$

$$C_S = -0.00092\text{mm}^{-1}, \tag{3.3.22c}$$

$$A = 0.4340\text{mm}^{-2}, \tag{3.3.22d}$$

$$D = -4.17\text{x}10^{-5}\text{mm}^{-4}. \tag{3.3.22e}$$

These values result in 0.0λ of spherical aberration and 0.0λ of coma. Much better performance is expected with the hybrid than with a conventional doublet because a

fourth-order phase coefficient was used. The equivalent for the conventional doublet would be to use an aspheric surface. While this would greatly increase the complexity of the conventional doublet, a fourth-order phase coefficient can be added to the diffractive surface without significantly increasing fabrication difficulties.

Comparing the above equations with Eqs. (3.3.16a) reveals one of the advantages of hybrid achromats. While C_{11}, the curvature on the front surface of the BK7 element, is almost the same for both achromats, the second curvature of the BK7 element in the hybrid example is about 35 times lower than its conventional counterpart. The weight of the hybrid achromat will likewise be reduced since there is no negative element. Additionally, the BK7 component of the hybrid contains about a third of the power contained in the BK7 element of the conventional achromat, which will make the hybrid lighter as well.

So far, all of the analysis involving spherical and coma has taken place at one wavelength. As seen in Eq. (2.2.13), however, the power of a diffractive element has a strong linear dependence on incident wavelength, or in other words,

$$\phi_2 = \frac{\lambda \phi_0}{\lambda_0}, \tag{3.3.23}$$

where λ is the incident wavelength, λ_0 is the design wavelength, and ϕ_0 is the design focal length. Substituting the above expression, along with Eq. (3.3.20) and Eq. (3.3.19) into

$$\begin{aligned} S_{II} + S_{I2} &= S_{I,tot} \\ &= \frac{y_1^4 \phi_1^3}{4}\left[a_1 B_1^2 + b_1 B_1 T_1 + c_1 T_1^2 + d_1\right] + \frac{y_2^4 \phi_2^3}{4}\left[B_2^2 + 4B_2 T_2 + 3T_2^2 + 1\right] - 8\lambda D y^4 \end{aligned}, \tag{3.3.24}$$

where $S_{I,tot}$ is the total spherical aberration in the achromat, allows us to find an expression for the amount of spherochromatism present. Making the above substitutions, the result is

$$S_{IACH} = \frac{y^4}{4}\left\{\phi_1^3\left[\left[a_1(\lambda)B_1^2 + b_1(\lambda)B_1T_1 + c_1(\lambda)T_1^2 + d_1(\lambda)\right]\left(\frac{n_1(\lambda)-1}{n_1(\lambda_0)-1}\right)^3 - \left[a_1(\lambda_0)B_1^2 + b_1(\lambda_0)B_1T_1 + c_1(\lambda_0)T_1^2 + d_1(\lambda_0)\right]\frac{\lambda}{\lambda_0}\right] + \phi_2^3\left(B_2^2 + 4B_2T_2 + 3T_2^2 + 1\right)\left(\frac{\lambda^3 - \lambda\lambda_0^2}{\lambda_0^3}\right)\right\}, \quad (3.3.25)$$

where ϕ_1 and ϕ_2 are the powers of the elements at the design wavelength. If $\lambda=\lambda_0$, Eq. (3.3.25) goes to zero, and the spherochromatism vanishes. The effect of spherochromatism on the performance of the hybrid achromat designed above can be seen in Fig. 3.3.4.

Trying to minimize the spherochromatism analytically quickly becomes a rather formidable problem. Since adding defocus to a system can offset the effects of spherical aberration, we are compelled to add some longitudinal chromatic aberration to offset the affects of spherochromatism. Equation (3.3.25), however, is extremely complicated. The coefficients a_1 - d_1 are all functions of wavelength, and the bending parameters B_1 and B_2 are functions of ϕ_1 and ϕ_2. Minimizing spherochromatism is perhaps better accomplished with the help of lens design software, just as designing real lenses from thin lens designs are likewise accomplished with the help of a computer.

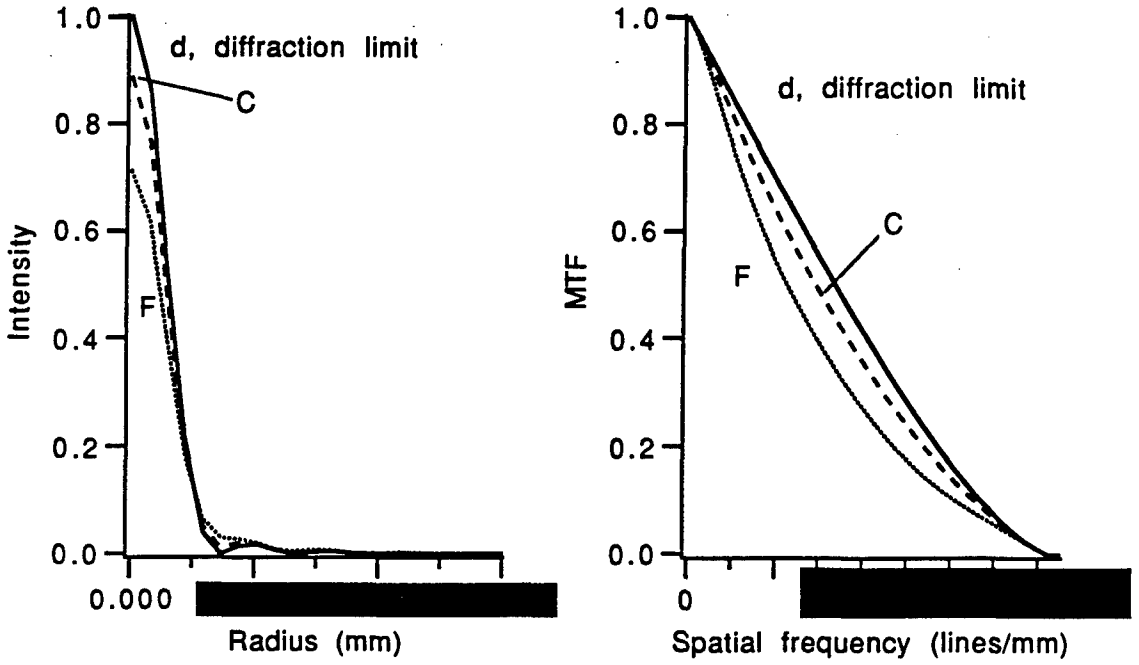

Fig. 3.3.4 Affect of spherochromatism on the PSF and MTF of a hybrid achromat. Plots of the PSF and MTF are shown for the F (0.4861μm), C (0.6563μm), and d (0.5876μm) wavelengths. Since there is no spherical aberration at the d wavelength, the plots for that wavelength coincide with the diffraction limit.

3.4. Summary of chapter 3

Since third-order thin lens solutions are often used as starting points in lens design, this chapter laid the foundation for the design of hybrid achromats. Section 3.2 showed that third order aberrations reduce the PSF and MTF of an achromatic doublet. When the two elements of a doublet are aligned correctly, the aberrations in one lens can be used to minimize aberrations in the other. Fabrication errors, such as decenter and tilt., may arise with systems having more than one lens element. If the elements are decentered or tilted with respect to one another, the aberrations do not cancel. It was also found that decenter and tilt will cause a shift in the image, and that this shift is proportional to the amount of error. For these reasons, it is advantageous, if possible, to correct aberrations as closely as possible to their origin.

In section 3.3, conventional and hybrid diffractive/refractive achromats were designed. Using equations presented in chapter 2, a method was presented for designing a cemented conventional achromat with minimal third order spherical aberration and coma. A solution could not be found for zero spherical and coma, since there are more constraints than degrees fo freedom, therefore a solution was chosen which yielded very small amounts of each. The process was then applied to the design of a hybrid achromat. The power required for achromatization by the diffractive surface was found to be quite low. For this reason a fourth order phase term needed to be used to minimize spherical aberration. With the addition of the fourth-order phase coefficient, there were enough degrees of freedom to find a solution with exactly zero spherical and coma. Less power in the BK7 element of the hybrid example resulted in lower surface curvatures as compared with the conventional doublet. Lower surface curvatures will in turn lower the weight of the lens. Finally the spherochromatism of the hybrid element was calculated and was found to reduce both the PSF and MTF as expected.

3.5 References for chapter 3

1. G. G. Sliusarev, "Optical systems with phase layers," Sov. Phys. Dokl **2,** 161-163 (1957).
2. A. Tudorovskii, "An objective with a phase plate," Opt. and Spect. **2,** 126-133 (1959).
3. K. Miyamoto, "The phase Fresnel lens," J. Opt. Soc. Am. **51,** 17-20 (1961).
4. H. Madjidi-Zolbanine, C. Froely, "Holographic correction of both chromatic and spherical aberrations of single glass lenses," Appl. Opt. **18,** 2385-2393 (1979).
5. T. Stone, N. George, "Hybrid diffractive-refractive lenses and achromats," Appl. Opt. **27,** 2960-2971 (1988).
6. D. Faklis, G. M. Morris, "Broadband imaging with holographic lenses," Opt. Eng. **28,** 592-598 (1989).
7. P. Twardowski, P. Meyrueis, "Design of some achromatic imaging hybrid diffractive-refractive lenses," *Holographic Optics III: Principles and Applications*, Proc. SPIE, **1507,** pp. 55-65 (1991).
8. R. Kingslake, *Lens Design Fundamentals* (Academic Press, San Diego, 1978), pp. 125-133.
9. W. J. Smith, *Modern Optical Engineering* (McGraw-Hill, New York, 1990), pp. 372-378.
10. W. T. Welford, *Aberrations of Optical Systems* (Hilger, Bristol, 1986), pp. 193-195,236-237.
11. J. W. Goodman, *Introduction to Fourier Optics* (McGraw-Hill, New York, 1968), pp. 102-110.
12. Reference 11, pp. 114.
13. Reference 11, pp. 122-125.

4. Optical data storage

4.1. Introduction

One application where a hybrid achromat may be particularly useful is in optical data storage (ODS) systems. Optical data storage systems record information on an optical disk by focusing light to a point, called the optical "stylus," and in some way altering the recording medium. *Access time* includes various mechanical delays and is defined as the time required to move the write/read head from one data location to another.[1] Making the head as small and light as possible decreases the access time. Included in the head are an objective lens and mechanisms that refocus and move the lens laterally to maintain a bright focus on the desired track.[2] The lens is relatively light, but its weight directly affects the size and weight of the refocusing mechanisms. Additionally, these mechanisms create more heat the harder they have to work. The objective lens, therefore, should be as small and light as possible.

The light source for ODS systems is a laser diode. As the ODS system switches from read to write mode, output power increases to a level sufficient to leave a mark on the recording medium. Corresponding to this increase in power, there is an increase in temperature and a shift in wavelength of approximately 3-4nm. There are also smaller shifts in wavelength due to mode hopping.[3] These wavelength changes alter the effective focal length of the objective lens, and occur much faster than the machine can refocus. One solution is to achromatize the objective lens. Conventional refractive achromats can be used, but as shown in Section 3.2, a hybrid achromat is much smaller and weighs considerably less.

In this research, a hybrid achromat has been designed for use in an optical data storage machine. Design constraints and performance goals are discussed in Section 4.2. Design constraints include field of view, f/number, entrance pupil diameter, and working distance. Performance goals are given in terms of a minimum polychromatic Strehl ratio

and a maximum achromatization limit. One quadratic and two sixteen-level diffractive surfaces are considered. Fabrication errors are discussed in Section 4.3. Errors which affect the Strehl ratio include element misalignment, thickness errors, and diffractive surface zone radii error. Errors which affect diffraction efficiency include blaze height and mask alignment errors.

4.2. Hybrid objective design

4.2.1. Design goals

Typical ODS objective lens dimensions are shown in Fig. 4.2.1. The entrance pupil radius is 4.3mm; the distance between the lens and the disk, or *working distance*, is between 1-2mm; and the f/number is less than or equal to 1.0. Light is focused through a 1.2mm polycarbonate protective layer onto the recording surface.[4] For mounting tolerance, a 1° half field of view is included. Design goals include keeping the polychromatic Strehl ratio at least 0.96 over the full field of view, and keeping the ratio of focal length change to wavelength change less than or equal to 0.1μm/nm. The design wavelength is 780±4nm.

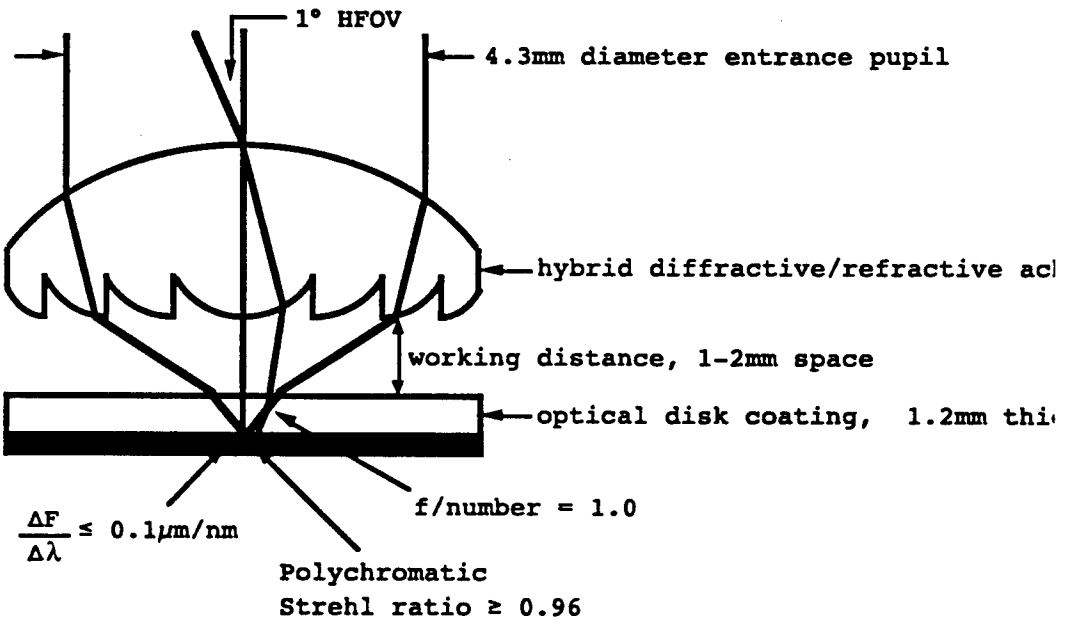

Fig. 4.2.1 Hybrid diffractive/refractive achromat used as an ODS objective. The entrance pupil diameter, field of view, and disk layer thickness are design restrictions; the working distance and f/number are variable; the Strehl ratio and achromatization ratio are design goals.

Using the thin lens model described in Section 2.3, a starting point for the achromat

was found. For fabrication reasons, the diffractive surface, and therefore the second surface of the refractive element, was kept flat. Keeping this surface flat deviates from the design process described in Section 3.3 because it removes two degrees of freedom. If the design process is followed, however, the resulting shape is nearly convex-plano, the nominal shape for a singlet with minimal third-order spherical and coma.[5] Although the hybrid achromat is not a singlet, nearly all of the power for the achromat is in the refractive element, as seen in Eq. (3.3.22d). Restricting the diffractive element to a flat surface does not introduce significant aberrations.

To achieve the desired performance, the first surface of the refractive element was made aspheric, and higher order phase terms were included in the diffractive surface. Monochromatic performance was optimized by minimizing the RMS spot size at 0°, 0.7°, and 1° fields of view. Achromatization was achieved by tracing rays at the extremes of the wavelength band, $\Delta\lambda$ = 766–784nm, and then minimizing the difference between their image plane location and that of the design wavelength, λ_0 = 780nm.

The resulting achromat is a convex–plano lens with an entrance pupil diameter of 4.3mm, a working distance of 1.92mm, and an f/number of 1.00. The polychromatic Strehl ratio is greater than 0.97 over the full field, as shown in Fig. 4.2.2.. and the focal length change per wavelength change is less than 0.023μm/nm.

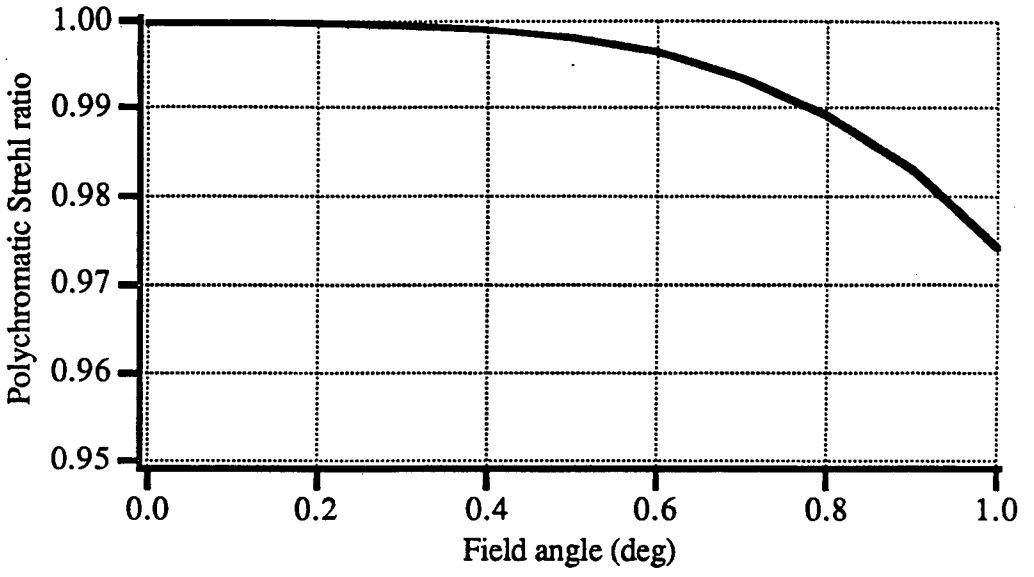

Fig. 4.2.2. Polychromatic Strehl ratio vs field angle. The lens was designed with a half field of 1° to account for errors introduced when mounting the lens into the ODS head.

The diffractive surface has the phase function shown in Fig. 4.2.3. The left axis is marked off in units of 2π phase cycles, so that the edge of a new zone is located wherever the line moves through an integer on the left axis. From the plot, then, we see that there are 53 zones in the diffractive element. As shown in Fig. 4.2.1, however, light entering the lens bends inward, so that the zones at the edge of the diffractive lens are never used. In fact, light will pass through only 20 zones. The width of the first and largest zone is 314.1μm, and the width of the smallest zone, near the edge of the element, is 18.6μm. The width of the zone 20, the smallest used zone, is 32.4μm. The focal length of the diffractive surface is 62.5mm and its f/number is 14.5.

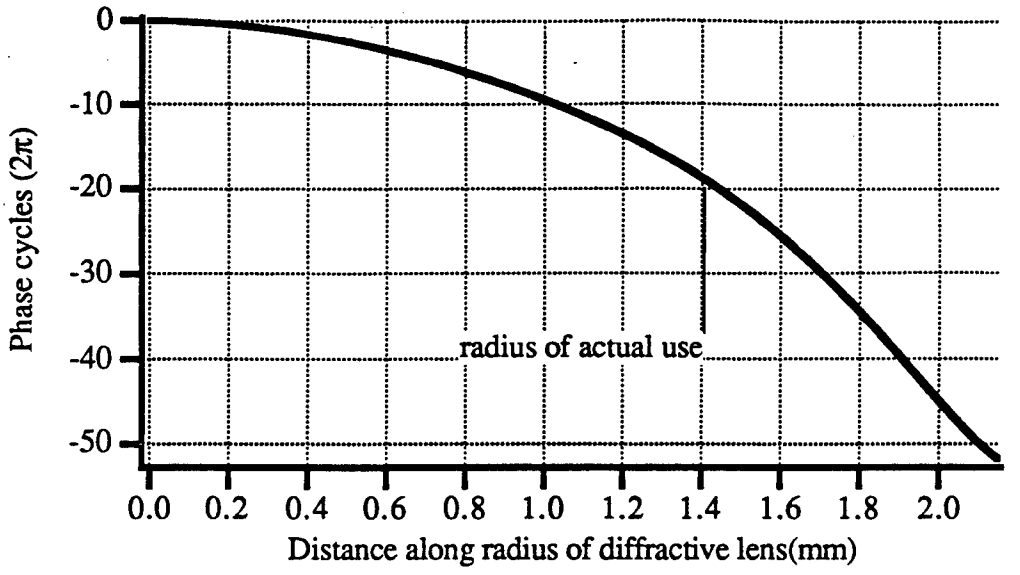

Fig. 4.2.3 Phase function for the diffractive element. The distances where the plot moves through another phase cycle mark the radii of the zones.

4.2.2. Fabrication

The refractive element will be injection molded, and the diffractive surface will then be bonded onto, or etched into, the flat surface of the refractive element. Three different methods will be used to fabricate one quadratic and two sixteen–step profiles.

The quadratic profile will be diamond turned into a layer of PMMA that has been bonded onto the flat surface of the refractive lens, as shown in Fig. 4.2.4. The diffraction efficiency of this lens is given by Eq. (2.2.16). With a quadratic blaze, and neglecting errors, 100% of the incident light diffracts into the first order.

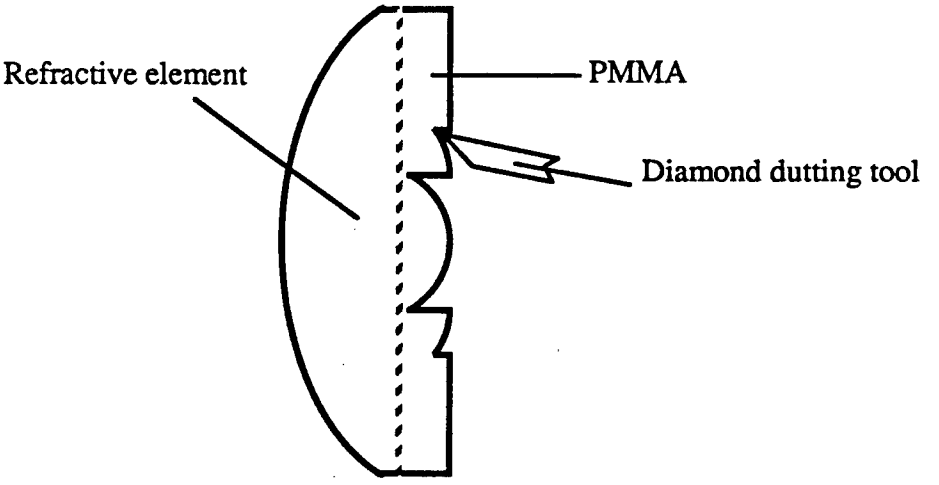

Fig. 4.2.4. Quadratic blaze profile being constructed with a diamond turning lathe. The material for the diffractive element will be PMMA, and bonded onto the refractive piece prior to cutting.

Two sixteen–level elements will be fabricated. One multilevel diffractive surface will be ion milled directly into the back surface of the refractive element, as in Fig. 4.2.5.

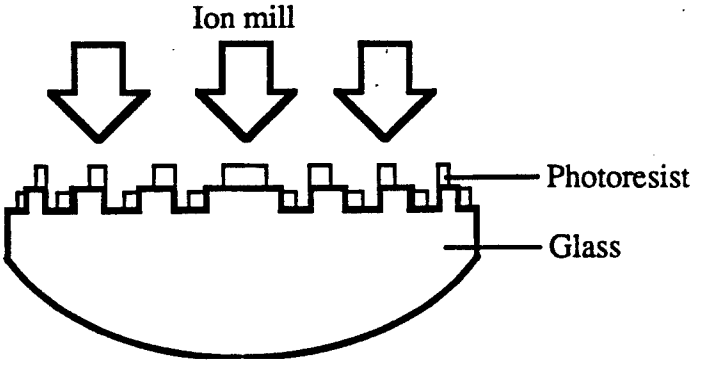

Fig. 4.2.5. Ion milling a diffractive element into the flat surface of a refractive element. A total of four etch cycles will be used to produce a sixteen-level diffractive element.

Another sixteen-level element will be etched into silicon. This surface will then be used to produce a mold, which can in turn be used to replicate the diffractive surface onto many refractive elements. This replication process is very similar to procedures that are currently used to make aspheric coatings on spherical glass surfaces.[6–11] After the flat surface of the refractive element is coated with a material, such as UV-curing epoxy or a plastic for example, the mold is pressed into this layer and the material is hardened. The mold is then removed, leaving the desired diffractive surface. The process is shown in Fig. 4.2.6.

Using Eq. (2.2.19), the maximum diffraction efficiency for a profile with $p = 16$, $\alpha = 1$, and $m = 1$, is approximately 98.7%. The effects of fabrication errors is discussed in the following section.

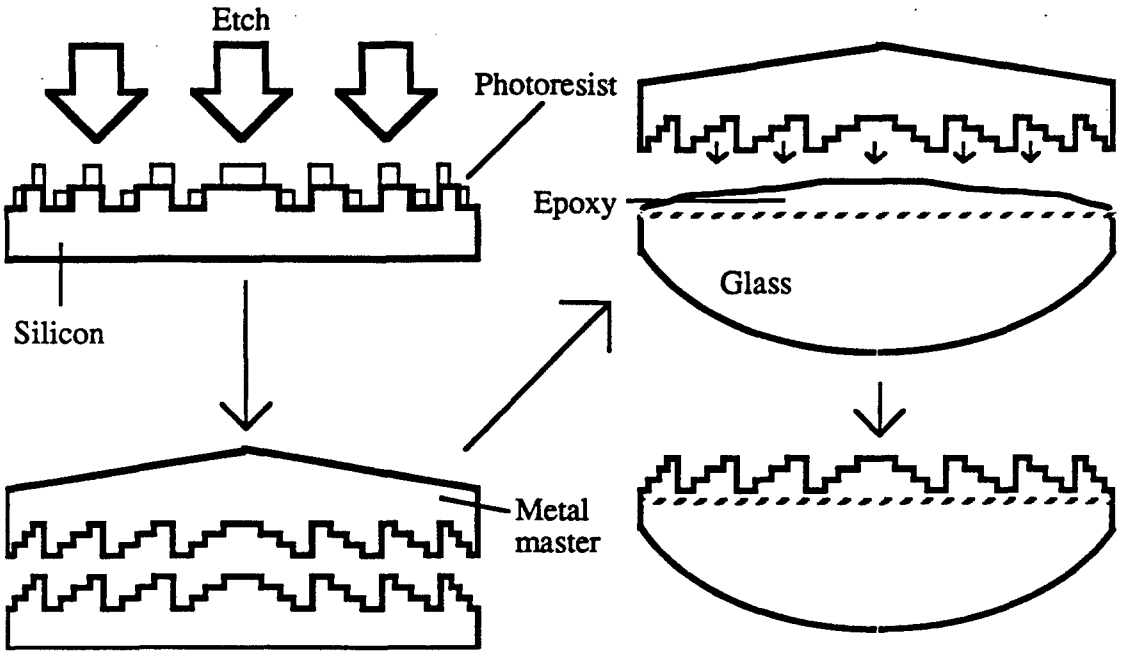

Fig. 4.2.6. Making a master for replication. The desired surface profile is first etched into silicon, and this surface is used to produce a master out of metal. Using a material such as epoxy, the master can then be used to replicate the diffractive surface onto many refractive elements. For simplicity, only four-levels are shown.

4.3. Fabrication tolerances

4.3.1. Image quality

It is important to consider how the achromat would perform with fabrication errors such as element misalignment, thickness error, and zone radii shrinkage. These errors will affect the achromats image quality, but not its diffraction efficiency. Element misalignment includes decenter and tilt, discussed more generally in Section 3.2.2, and shown in Fig. 4.3.1. The design should be able to work well out to ±10μm of decentering and ±0.2° of tilt. The effects of these fabrication errors is shown in Figs. 4.3.2 and 4.3.3.

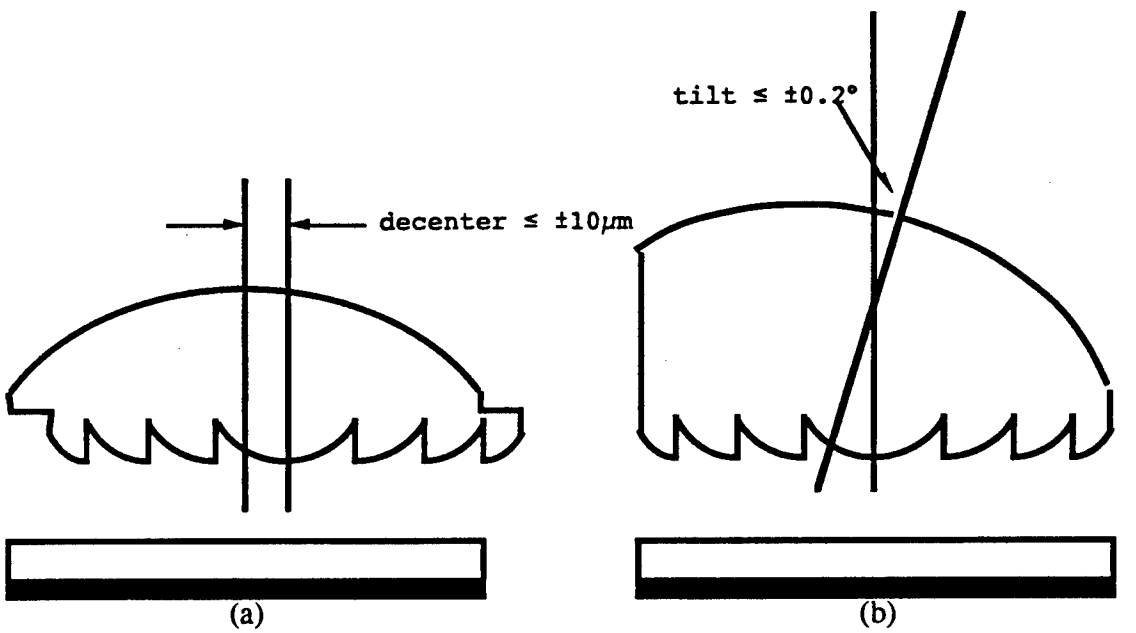

Fig. 4.3.1. Decenter and tilt. The design should perform well with up to ±10μm decenter and ±0.2° tilt.

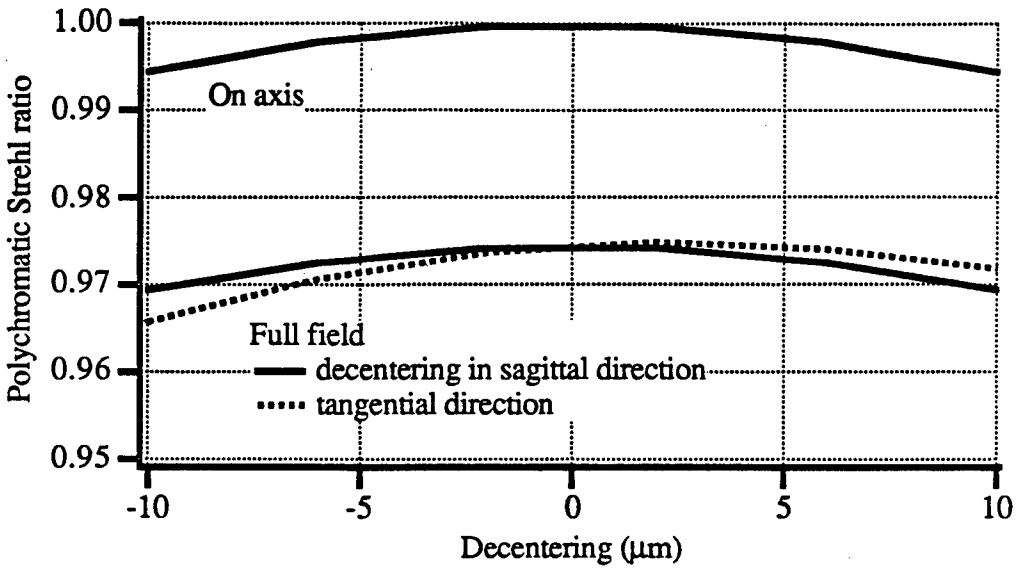

Fig. 4.3.2. Polychromatic Strehl ratio vs decentering. On axis, the Strehl ratio stays greater than 0.99 over the desired range. Even at full field, the Strehl ratio stays above 0.96.

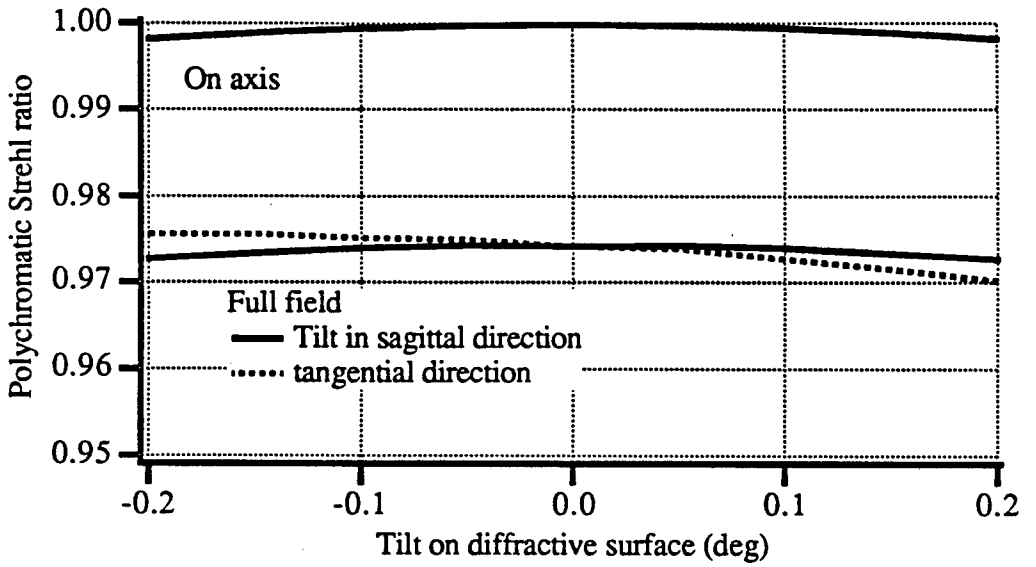

Fig. 4.3.3. Polychromatic Strehl ratio vs tilt. Tilt of only ±0.2° does not have much of an effect on the Strehl ratio. On axis, the Strehl ratio is higher than 0.99, and at full field it stays above 0.97.

In addition to decenter and tilt, there can also be an error in the thickness of either the refractive or diffractive element, as in Fig. 4.3.4. This does not include error in the thickness of the surface relief pattern itself, which affects only diffraction efficiency.

Thickness error in the refractive element or substrate will affect the Strehl ratio in a manner shown in Fig. 4.3.5. Because the common surface is flat, the effect of thickness error in each element is very similar. To maintain a Strehl ratio greater than 0.96, the thickness errors cannot be greater than ±25μm.

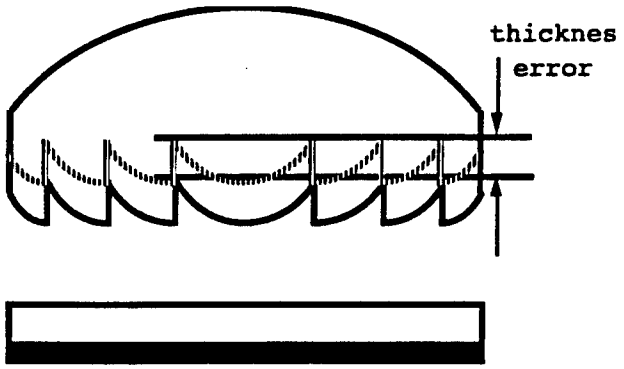

Fig. 4.3.4. Thickness error. Blaze height error affects the diffraction efficiency and discussed in the next section.

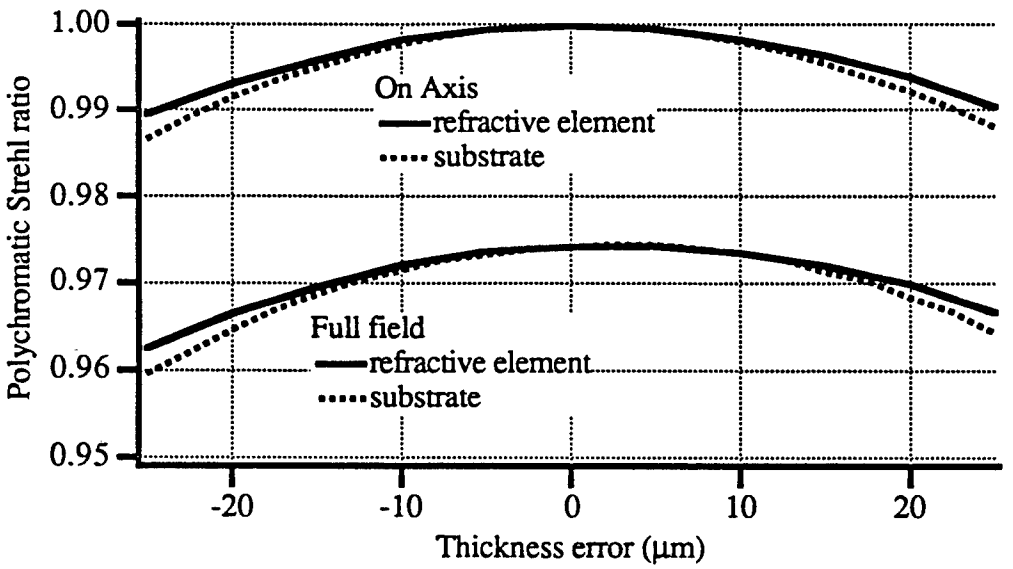

Fig. 4.3.5. Polychromatic Strehl ratio vs substrate or refractive element thickness error. To maintain the desired Strehl ratio, the thickness error must be kept under 25μm.

Zone shrinkage or expansion, shown in Fig. 4.3.6, is another error that will degrade the performance of the lens. If the diffractive surface is made from plastic or an epoxy, for example, the radii of the zones will change as the surface shrinks and expands with

temperature. In Section 2.2.1, we saw that changing the zone radii effectively changes the focal length of the diffractive element. The ODS objective, however, utilizes higher order phase coefficients, and changing the zone radii by even 1% will greatly degrade the wavefront, and will have a detrimental effect, as seen in Fig. 4.3.7. To maintain a Strehl ratio above 0.96, the zone shrinkage and expansion must be under ±0.7%. Fortunately the diffractive surface is bonded onto, or blazed into, a more stationary glass surface. If the diffractive surface shrinks or expands, the most significant change will be in the surface height.

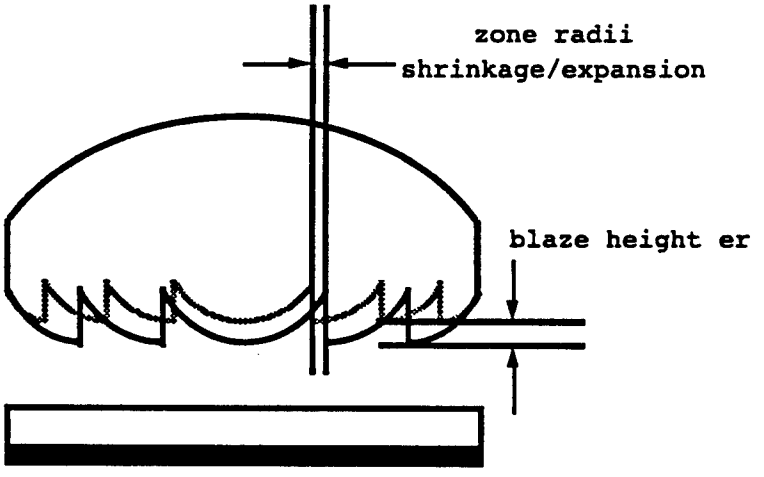

Fig. 4.3.6. Diffractive surface shrinkage and expansion. Both the zone radii and surface height are affected. The effect of height error on diffraction efficiency is discussed in Section 4.3.2.

A change in the focal length of the diffractive surface will also affect the achromatization of the lens. A goal of the design was that the ratio of focal length change to wavelength change should not exceed 0.1μm/nm. As seen in Fig. 4.3.8, expanding the zones by as much as ±5% does not exceed the 0.1μm/nm limit. Shrinking the zones actually improves the achromatization, but at the cost of monochromatic performance.

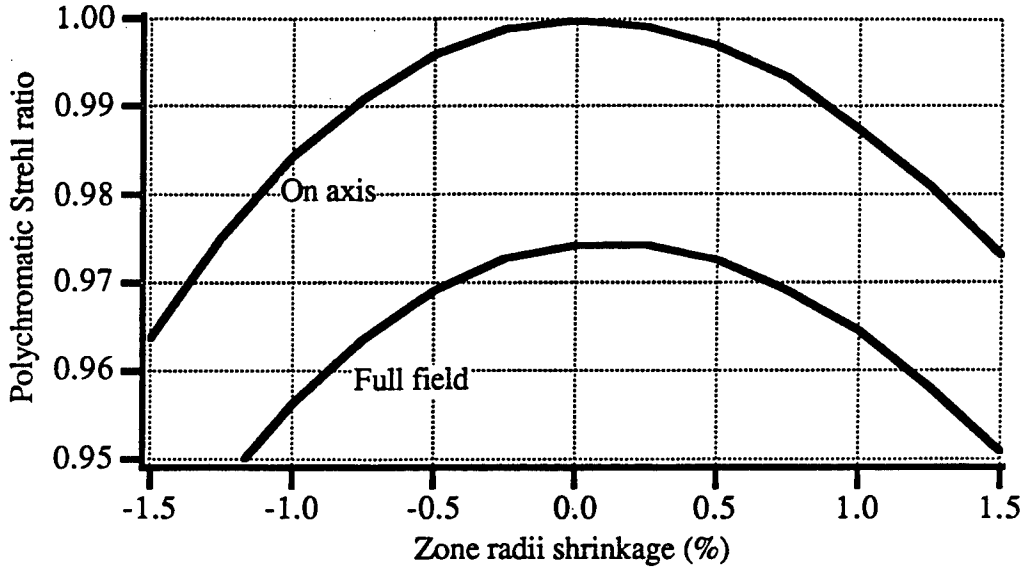

Fig. 4.3.7. Polychromatic Strehl ratio vs zone radii shrinkage. To keep the Strehl ratio higher than 0.96 at full field, shrinkage should be kept under ±0.7%.

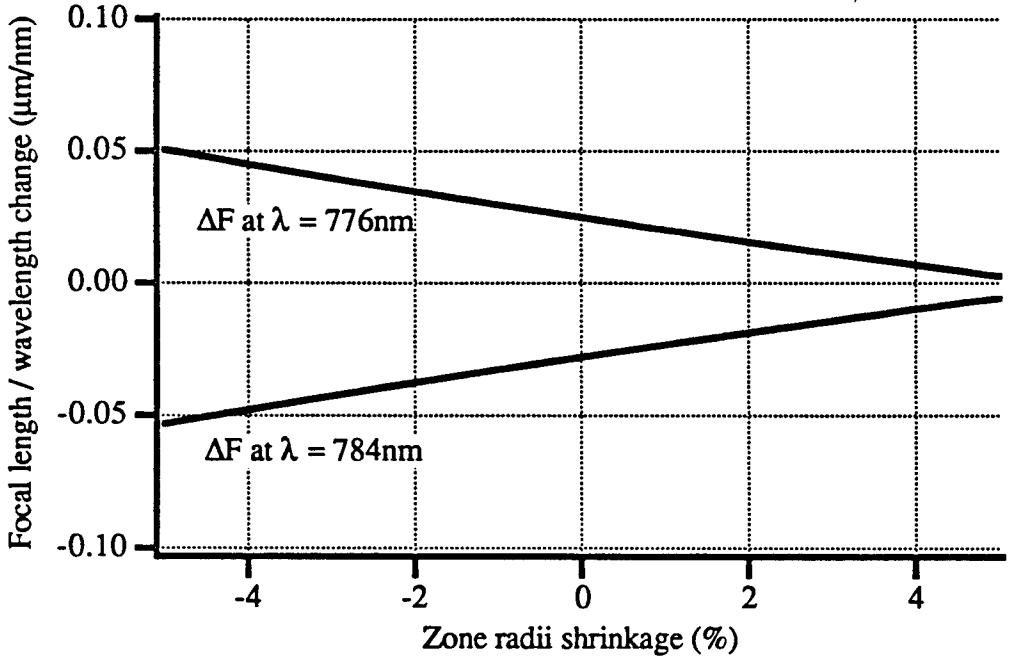

Fig. 4.3.8. Focal length per wavelength change vs zone radii shrinkage. Even if the shrinkage is greater than ±5%, the lens is achromatized within the 0.1μm/nm limit.

In the discussion above, all of the errors were treated individually. Actually, of course, there will be a combination of errors. Fig. 4.3.9 provides predicted polychromatic

Strehl ratios for the four cases listed in Table 4.3.1. Since zone shrinkage is likely to be extremely low, values are included assuming no change in zone radii.

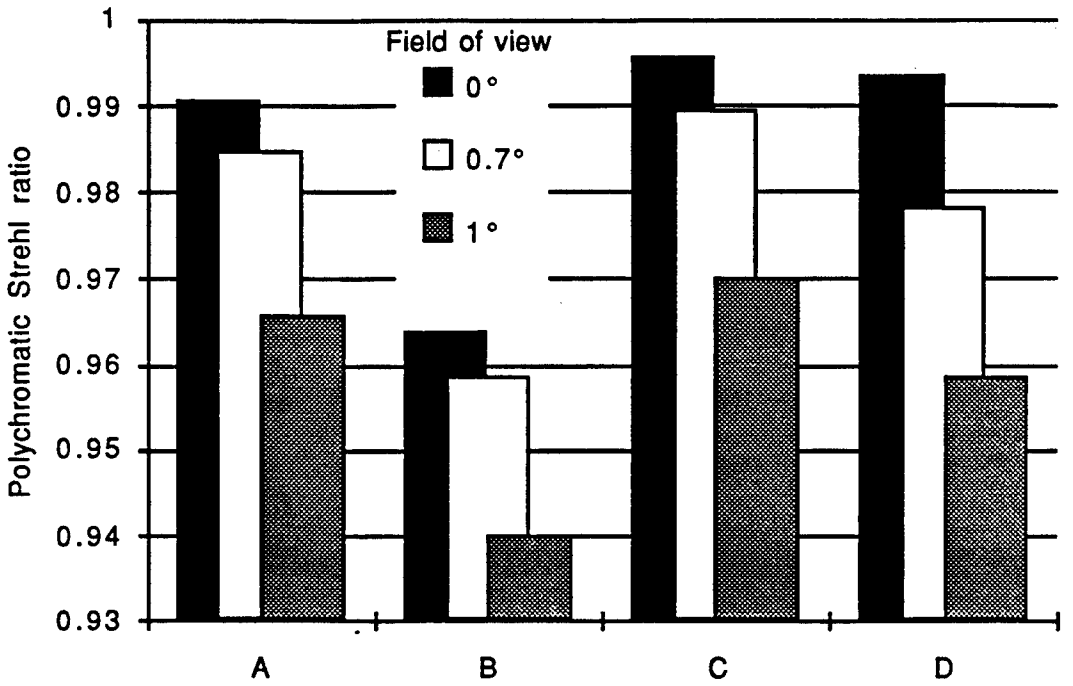

Fig. 4.3.9. Polychromatic Strehl ratios for the four cases listed in Table 4.3.1.

Columns	Decenter (μm) (sagittal)	Tilt (deg) (sagittal)	Thickness (μm)	Zone radii (%)
A	5	0.1	12.5	0.35
B	10	0.2	25	0.7
C	5	0.1	12.5	0
D	10	0.2	25	0

Table 4.3.1. Four different combinations of fabrication errors.

As seen in Fig. 4.3.9, assuming zone radii changes are negligible, the Strehl ratio dips below 0.96 only in the worst case scenario. If the field angle tolerance can be kept under 1° half field of view, however, acceptable performance can be expected.

4.3.2. Diffraction efficiency

Errors such as blaze height and mask alignment affect the shape of the surface blaze, hence they do not introduce aberrations to the lens, rather, they lower the diffraction efficiency. Farn and Goodman,[12] and Cox, et. al.[13, 14, 15] investigated the effects of etch depth error on the image quality and diffraction efficiency of two-level diffractive lenses, and the effects of mask misalignment error on four-level diffractive lenses. Cox, et. al. found that *within the capabilities of current technology*, neither of these fabrication errors had a significant impact on image quality, and only mask alignment error would significantly reduce the diffraction efficiency. Nevertheless, it is still useful to investigate the causes and effects of depth error as well as mask alignment error.

In Section 4.3.1, for example, material shrinkage and expansion were presented as reasons for changes in zone radii. Because the diffractive element is bonded onto a glass surface, however, if the material shrinks or expands, almost all of the change will be in the thickness of the surface, introducing a depth error. Diffraction efficiency as a function of order number and surface blaze height can be found with the help of Eq. (2.2.3), which expresses the phase introduced by a diffractive lens as

$$\varphi(r) = \left(\frac{2\pi}{\lambda}\right)\left[n_s(\lambda) - 1\right]d(r), \tag{4.3.1}$$

where n_s is the refractive index of the substrate material and d(r) is the height of the blaze

at the radius r. If λ_o is the design wavelength, and $d_0(r)$ is the design thickness, then the desired phase modulation is

$$\varphi_0(r) = \left(\frac{2\pi}{\lambda_o}\right)\left[n_s(\lambda_o) - 1\right]d_0(r). \tag{4.3.2}$$

Combining Eqs. (4.3.1) and (4.3.2) yields

$$\varphi(r) = \alpha\varphi_0(r) \tag{4.3.3}$$

where

$$\alpha = \frac{\lambda_0}{\lambda}\frac{\left[n_s(\lambda) - 1\right]}{\left[n_s(\lambda_o) - 1\right]}\frac{d(r)}{d_0(r)}. \tag{4.3.4}$$

Setting $d = d_o$ results in the definition for α given by Eq. (2.2.6). If we assume that $\lambda = \lambda_o$, then alpha is given by

$$\alpha = \frac{d(r)}{d_0(r)}. \tag{4.3.5}$$

Substituting this into Eq. (2.2.16) gives us the following expression for a quadratic blaze:

$$\eta(d, m) = \mathrm{sinc}^2\left(\frac{d}{d_0} - m\right). \tag{4.3.6}$$

For a multi-level diffractive lens, using Eq. (2.2.18), the equivalent relationship is

$$\eta(d, p, m) = \frac{\sin^2\left(\frac{\pi m}{p}\right)\sin^2\left[\pi\left(\frac{d}{d_0} - m\right)\right]}{(\pi m)^2\sin^2\left[\frac{\pi}{p}\left(\frac{d}{d_0} - m\right)\right]}, \tag{4.3.7}$$

where p is the number of levels. Equations (4.3.6) and (4.3.7), with p = 16, are shown in Fig. 4.3.10.

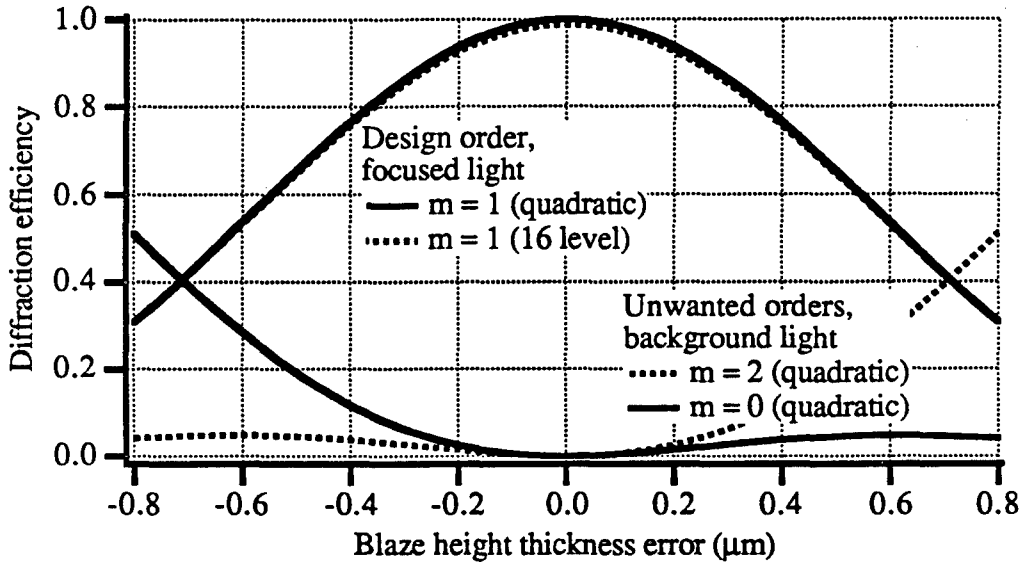

Fig. 4.3.10. Diffraction efficiency vs blaze height thickness error. The design order is the first order. Other orders, when $d \neq d_o$, give rise to background light.

Unfortunately, most fabrication errors are extremely difficult to model. For example, a sixteen-level diffractive lens requires four mask and etch steps, and each etching will generate a different error. Each step will therefore have it's own α_k as given by Eq. (4.3.5). The phase of a p level diffractive lens, given by Eq. (2.2.17), will then take the form,

$$\varphi(r) = \frac{2\alpha_k \pi}{p}(p+k), \tag{4.3.8}$$

where α_k is no longer a constant. If d_o is the maximum thickness, then the design height of the k^{th} level is given by $d_{ok} = d_o - (k/p)d_o$ and the actual height is given by $d_k = d_{ok} - \Delta_k$, where Δ_k is the step error. Substituting these heights into Eq. (4.3.5) and simplifying, we find that α_k is given by

$$\alpha_k = 1 + \frac{p\Delta_k}{d_0(p-k)}. \qquad (4.3.9)$$

Assuming the profile is made with 2^n steps, which is most often the case, it's easy to quickly calculate Δ_k as a function of etch error, δ_n, with the help of a "binary code." The procedure is shown in Fig. 4.3.11.

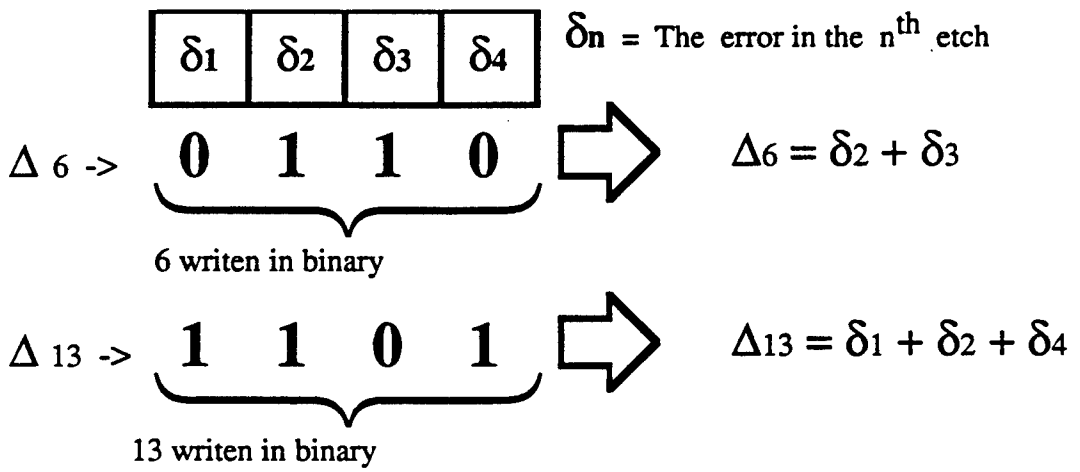

Fig. 4.3.11. "Binary code" used to quickly calculate Δ_k. In this example, four masks for a sixteen-level diffractive lens is assumed.

The example above is for a four mask, or sixteen-level diffractive lens. Each of the etches will have it's own etch error, δ_n. Each step error, Δ_k, will be some combination of δ_n. To find the correct combination, the etch errors are pictorially placed next to each other, as in Fig. 4.3.11. The value of Δ_6, for example, is found by writing "6" in binary, 0110, with one digit under each etch error. The etch errors above the 1's, δ_2 and δ_3, will sum to Δ_6. This method provides a quick way of calculating Δ_k, and α_k, which is especially useful in computer programs.

Now that α_k is defined, the procedure given in Chapter 2 is used with Eq. (4.3.8), to find the following expression for the diffraction efficiency,

$$\eta(p,m)=\left|\frac{\sin\left(\frac{\pi m}{p}\right)}{\pi m}\sum_{k=0}^{p-1}\exp\left[\frac{i2\pi}{p}\left[\alpha_k(p+k)-km\right]\right]\right|^2, \qquad (4.3.10)$$

where, as before, m is the order number and p is the number of steps.

Expanding Eq. (4.3.10) with two levels is simple, with four levels is tedious, and with eight or more levels is likely to produce mistakes. To calculate diffraction efficiency for a sixteen-level lens, a program was written which calculated α_k, performed the summation, and multiplied by the complex-conjugate. The results for various combinations of etch errors are shown in Table 4.3.2.

case	δ 1	δ 2	δ 3	δ 4	η
1	0	0	0	0.08881	0.950
2	0	0	0.177625	0.08881	0.811
3	0	0	0	0.07	0.964
4	0	0	0.07	0	0.964
5	0	–0.07	0	0	0.964
6	–0.07	0	0	0	0.964
7	0	0	0.07	–0.07	0.941
8	0.07	–0.07	0	0	0.941
9	–0.1	0.1	–0.1	0.1	0.811
10	0.1	0.1	0.1	–0.1	0.811
11	0.1	–0.09	–0.21	0.001	0.722
12	–0.001	0.21	0.1	–0.09	0.722

Table 4.3.2 Diffraction efficiencies for various etch depth errors.

The maximum height of the profile used in Table 4.3.2 is 1.421μm, which the design height of the profile to be made of epoxy. Cases 1 and 2 are provided to check the calculations. Case 1 shows that if the fourth etch step is off by a complete step height, essentially making the sixteen-level lens an eight-level lens, then the diffraction efficiency is that of an eight-level lens. Case 2 is similar, but now the third etch step is off by two step heights, resulting in the diffraction efficiency of a four-level lens. Cases 3-6 show that the origin and sign of the error are irrelevant. This is also seen in cases 7 and 8, and cases 9 and 10, where different combinations of equal errors result in the same efficiencies. Finally, 11 and 12 show that even different combinations of unequal errors of changing sign result in the same diffraction efficiency. Evidently only the magnitude and number of errors is relevant. Typically etch errors of less than or equal to 0.7μm are possible.

Cox, et.al.[13, 14, 15] calculated the effects of misalignment on the diffraction efficiency, the results of which are shown in Fig. 4.3.12. They then verified these results by fabricating and testing several four-level diffractive lenses.

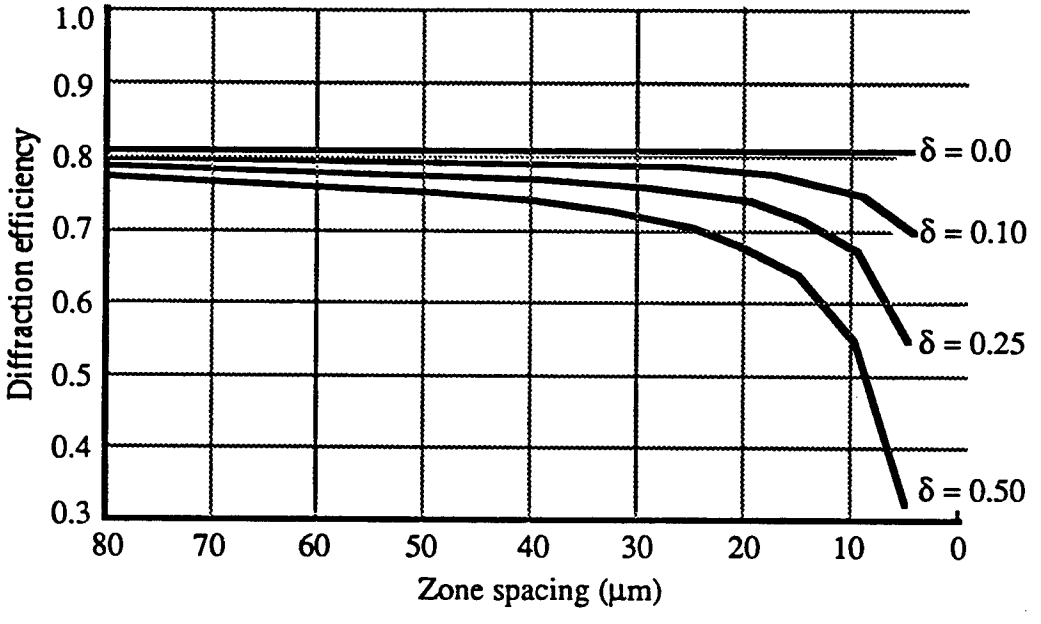

Fig. 4.3.12. The effects of misalignment by an amount δ on the diffraction efficiency of four-level f/10 diffractive lenses.

Alignment accuracy of less than 0.1μm is possible, but again, the results in Fig. 4.3.12 are for a four-level surface. A sixteen-level surface is much more complicated because each mask will contribute its own alignment error. Furthermore, with alignment errors, the lens is no longer circularly symmetric.

Exactly how non-unity diffraction efficiency will affect ODS systems is not yet known. It may be helpful, however, to examine the integrated efficiency, discussed in Section 2.2.2. Equation (2.2.25) shows that the integrated efficiency acts as a scaling factor for the MTF. Since the MTF and PSF of an optical system are Fourier transform pairs, the integrated efficiency also scales the PSF. However, unlike aberrations, which reduce the peak value of the PSF and increase the energy in the side lobes, energy lost from the peak value of the PSF due to non–unity diffraction efficiency is spread more or less uniformly across the image plane.

For the sixteen-level ODS lens discussed in Section 4.2, for example, the peak diffraction efficiency, assuming no fabrication errors, is 98.7%. Since the f/number of the diffractive lens is 14.5, scalar diffraction theory is assumed to be valid and the efficiency is constant across the surface of the element. Assuming monochromatic light and no fabrication errors, the integrated efficiency is then equal to the scalar diffraction efficiency, or 98.7%. 1.3% of the light in the PSF of the achromat, therefore, will be spread across an area at least 4mm in diameter. Since the achromat works at f/1.0 with $\lambda_0 = 0.780\mu m$, the optical stylus, or the light contained within the first zero of the Airy disk, has a diameter of 0.001903mm. The undiffracted light is therefore spread over an area many orders of magnitude larger than the optical stylus, and will most likely be negligible.

The reason the background is so diffuse is that with a sixteen-level diffractive lens, where the design order is m = 1, we see from Eq. (2.2.19) that the closest non-zero orders are m = -15, and m = 17, which illuminate an extremely large area. Even with

polychromatic light and fabrication errors, where light propagates into the m = 0 and m = 2 orders, background light illuminates an area 0.2mm in diameter, which is still orders of magnitude larger than the optical stylus. Whether this undiffracted light will have a significant impact an ODS system has yet to be determined.

4.4 Summary of chapter 4

In this chapter, we discussed one application of diffractive lenses, to achromatize an optical data storage objective. Section 4.2 outlined the design constraints and performance goals, and then presented the final result. A hybrid diffractive/refractive achromat was designed with a 4.3mm entrance pupil diameter, 1° half field of view, 1.9mm working distance, and an f/number of 1.00. The polychromatic Strehl ratio was shown to be greater than 0.97 over the full field, and the focal length change per wavelength change was shown to be less than 0.03μm/nm. The convex-plano refractive element is to be injection molded and made of glass. Three diffractive surfaces, one quadratic and two with sixteen-level profiles, will be fabricated.

Section 4.3 described how the lens would perform with certain fabrication errors. First errors that affected image quality were discussed. The lens performed acceptably with ±10μm decentering, 0.2° tilt, 25μm of thickness error, and 0.7% zone radii change, all of which are within capabilities of current technology. The combination of each of the errors at their maximum, an unlikely situation, degraded the Strehl ratio enough to dip beneath 0.96 at full field. Zone radii shrinkage or expansion, which affects the focal length of the diffractive surface, was also shown to have a negligible impact on achromatization. Errors which affected diffraction efficiency were then discussed. It was found that with etch depth errors, only the magnitude and number of errors is significant. Since it is not yet known how unwanted orders will affect the performance of ODS systems, it is difficult to specify a minimum required diffraction efficiency. Within the capabilities of current technology, etch depth errors can be kept negligibly small, but mask misalignment may be a problem.

4.5. References

1. A. B. Marchant, *Optical Recording: A Technical Overview* (Addison-Wesley, New York, 1990), p. 15-17.
2. Reference 1, pp. 202-208.
3. Reference 1, pp. 146-154.
4. Reference 1, pp. 102,126.
5. R. Kingslake, *Lens Design Fundamentals* (Academic Press, San Diego, 1978), pp. 118, 165-166.
6. H. Howden, J. A. Clarke, "Refracting replica aspheric optics," Opt. Eng. **15,** 197-201 (1976).
7. S. D. Fantone, "Replicating optical surfaces using UV curing cements," Appl. Opt. **22,** 764 (1983).
8. R. J. M. Zwiers, G. C. M. Dortant, "Aspherical lenses produced by a fast high-precision replication process using UV-curable coatings," Appl. Opt. **24,** 4483-4488 (1985).
9. D. Visser, T. G. Gijsbers, R. A. M. Jorna, "Molds and measurements for replicated aspheric lenses for optical recording," Appl. Opt. **24,** 1848-1852 (1985).
10. W. E. Asher, "Epoxy replication–advantages and limitations," *Replication and Molding of Optical Components*, Proc. SPIE, **896,** pp. 2-5 (1988).
11. G. B. A. Hut, J. W. Versluis, "Replicated aspheres meet optical memory needs," Laser Focus World **?,** 105-113 (1989).
12. M. W. Farn, J. W. Goodman, "Effect of vlsi fabrication errors on kinoform efficiency," *Computer and Optically Formed Holographic Optics*, Proc. SPIE, **1211,** pp. 125-136 (1990).

13. J. A. Cox, et al., "Diffraction efficiency of binary optical elements," *Computer and Optically Formed Holographic Optics*, Proc. SPIE, **1211**, pp. 116-123 (1990).

14. J. A. Cox, B. S. Fritz, T. R. Werner, "Process error limitations on binary optics performance," *Computer and Optically Generated Holographic Optics*, Proc. SPIE, **1555**, pp. 80-88 (1991).

15. J. A. Cox, B. Fritz, T. Werner, "Process-dependent kinoform performance," *Holographic Optics III: Principles and Applications*, Proc. SPIE, **1507**, pp. (1991).

5. Conclusion

The purpose of this thesis was to address the use of a hybrid diffractive/refractive achromat in optical data storage. Chapter 2 presented the tools needed to design an achromat with a diffractive element. Section 2.2 addressed rotationally symmetric diffractive lenses and included a discussion on diffraction efficiency, an additional concern that is not an issue with conventional refractive systems. When designing systems with diffractive elements, it may be advantageous to model the diffractive surface as a thin lens with an extremely high refractive index. Section 2.3 reviewed the thin lens, and showed how the aberrations of a diffractive surface can be considered a special case of the thin lens aberrations.

Chapter 3 was concerned with the design of achromatic doublets. The traditional method of designing a conventional refractive achromatic was first presented, then, using the thin lens model described in Chapter 2, a hybrid achromat was designed. The large negative dispersion of a diffractive lens, allowed the hybrid achromat to be formed of two positive elements. The refractive element of the hybrid was found to have lower surface curvatures than refractive elements in conventional doublets, resulting in much smaller and lighter achromats.

The application of hybrid achromats to optical data storage was presented in Chapter 4. A hybrid achromat is desirable because of its small size and light weight. It was seen that the hybrid achromat exceeded the design goals, and toleranced well with fabrication errors. Fabrication inaccuracies which decreased the diffraction efficiency were also investigated. One will be quadratic and two sixteen-level profiles are being investigated for the diffractive surface. Unfortunately, it is not yet known how the non-unity diffraction efficiency of the multi-level profiles will affect the performance of an optical data storage machine. The undiffracted light total a few percent at most and is extremely out of focus. While this background light shouldn't present a problem, a definite answer may not be known until the system is tested.